



ENGINEERING RESEARCH CENTER FOR
STRUCTURED ORGANIC PARTICULATE SYSTEMS
RUTGERS UNIVERSITY
PURDUE UNIVERSITY
NEW JERSEY INSTITUTE OF TECHNOLOGY
UNIVERSITY OF PUERTO RICO AT MAYAGÜEZ



Graz, University of Technology in Cooperation with Rutgers, State University of New Jersey

Understanding roller compactor process parameters by monitoring physical changes with near infrared spectroscopy

MASTER'S THESIS

Lukas Koller
Graz, June 2017

Supervisors:

Graz, University of Technology:

Ass.Prof. Dipl.-Ing. Dr.techn. Heidrun Gruber-Wölfler

Univ.-Prof. Dipl.-Ing. Dr.techn. Johannes Khinast

Rutgers, State University of New Jersey:

Dr. Douglas B. Hausner

Dr. Sara Moghtadernejad

Dr. Sarang Oka

Dr. Andrés David Román Ospino

Dr. James V. Scicolone

Dr. Fernando J. Muzzio

STATUTORY DECLARATION

I declare that I have authored this thesis independently, that I have not used other than the declared sources / resources, and that I have explicitly marked all material which has been quoted either literally or by content from the used sources.

.....

date

.....

(signature)

EIDESSTATTLICHE ERKLÄRUNG

Ich erkläre an Eides statt, dass ich die vorliegende Arbeit selbstständig verfasst, andere als die angegebenen Quellen/Hilfsmittel nicht benutzt und die den benutzten Quellen wörtlich und inhaltlich entnommene Stellen als solche kenntlich gemacht habe.

Graz, am

.....

(Unterschrift)

Abstract

The focus of this thesis is on density of roller compacted ribbons, and enabling its fast, accurate, representative and real time prediction using near infrared spectroscopy. This is because ribbon density has been shown to be a key predictor of granule properties post milling. Ribbons were created with the roller compactor BRC 25 from Bohle. Three unique, partial least square models (PLS) were developed using NIR spectra from two spectrometers, namely, Matrix-F from Bruker, (Fourier transform) NIR spectrometer and the JDSU MicroNIR. The Matrix F has many advantages over the smaller MicroNIR. However, the MicroNIR due its smaller size lends itself easily to being mounted online. A head-to-head comparison was thus made to evaluate the feasibility of using the MicroNIR for online monitoring of ribbon density. Calibration models were built. Tested materials were Avicel PH 102 and Prosolv. The Relative Standard Error of Prediction (RSEP) in % for Avicel PH 102 and Prosolv was 5,002 and 14,901, respectively. Since the calibration model built out of the MicroNIR values showed a RSEP of 9,284% for Avicel PH 102, which is almost the same value as it was for the models built out of the Matrix F values, only the values from the Matrix F were further analyzed for Prosolv. Ribbon density reference values for building the NIR models were made using GeoPyc from Micrometrics. Two alternate methods were also used to measure the ribbon density, namely estimating the ribbon volume by measuring its thickness using calipers and by estimating ribbon volume by measuring displacement of oil when it is inserted in an oil column. However, the other methods were found to be substantially less efficient and accurate compared to the GeoPyc measurements.

The results showed that in future it will be possible to save time and material by using PLS-models for predicting density of ribbons. Furthermore the RSEP of both NIR-spectrometers were comparable, which means that the small MicroNIR can also be used for online monitoring of ribbon density. In addition, the work provides a framework to create models for other process parameters so that the entire roller compactor process can be predicted without operating the machine itself.

Kurzfassung

Der Fokus dieser Arbeit liegt auf der Dichte von Walzen-komprimierten Bändern und ermöglicht die schnelle, genaue, repräsentative und Echtzeit-Vorhersage mit Nah-Infrarot-Spektroskopie. Dies liegt daran, dass die Banddichte ein wichtiger Prädiktor für die Granulat Eigenschaften nach dem Mahlen ist. Bänder wurden mit dem Walzenverdichter BRC 25 von Bohle geschaffen. Drei einzigartige, „partial least square“ Kalibrier - Modelle (PLS) wurden unter Verwendung von NIR-Spektren aus zwei Spektrometern entwickelt, nämlich mit der Matrix-F von Bruker, (Fourier Transformation) NIR Spektrometer und dem JDSU MicroNIR. Die Matrix F hat viele Vorteile gegenüber dem kleineren MicroNIR. Allerdings kann das MicroNIR aufgrund seiner kleineren Größe leicht, innerhalb des Walzenverdichters montiert werden. So wurde ein Kopf an Kopf Vergleich durchgeführt, um die Machbarkeit der Nutzung des MicroNIR zur Online-Überwachung der Banddichte zu bewerten. Kalibrier Modelle wurden gebildet. Getestete Materialien waren Avicel PH 102 und Prosolv. Der relative Standardfehler der Vorhersage (RSEP) in % für Avicel PH 102 und Prosolv betrug 5,002 bzw. 14,901. Da das aus den MicroNir Werten gebaute Kalibrier Modell, einen RSEP von 9.284% für Avicel PH 102 gezeigt hat, was fast der gleiche Wert war wie bei den Modellen die aus den Matrix F gebaut wurden, wurden nur die Werte des Matrix F für Prosolv weiter analysiert. Die Dichte Messungen der Bänder für den Aufbau der NIR Modelle wurden mit GeoPyc von Micrometrics durchgeführt. Es wurden auch zwei alternative Verfahren verwendet, um die Banddichte zu bestimmen, nämlich das Bandvolumen zu berechnen, indem die Dicke mit einem Messschieber gemessen wurde und indem die Verschiebung von Öl gemessen wurde, die durch hineinlegen der Proben in eine Öl Säule entstand. Allerdings waren die anderen Methoden im Vergleich zu den GeoPyc-Messungen wesentlich weniger effizient und genau.

Die Ergebnisse zeigten, dass es in Zukunft möglich sein wird, Zeit und Material zu sparen, indem PLS-Modelle zur Vorhersage der Dichte von Bändern verwendet werden. Darüber hinaus war der RSEP beider NIR-Spektrometer vergleichbar, was bedeutet, dass das kleine MicroNIR auch für die Online-Überwachung der Banddichte verwendet werden kann. Darüber hinaus bietet die Arbeit das Gerüst für die Erstellung von Modellen für andere Prozessparameter, so dass der gesamte Walzenverdichtungsprozess ohne Bedienung der Maschine vorhergesagt werden kann.

Table of Contents

Abstract.....	II
Kurzfassung.....	III
Table of Contents	IV
List of Figures	VII
List of Tables.....	X
1. Introduction	1
2. Roller Compactor	2
3. Density of roller compacted ribbons.....	3
3.1. Overview of different densities	3
3.2. Measurement of ribbon density	4
3.2.1. Caliper.....	4
3.2.2. Oil method	4
3.2.3. GeoPyc.....	5
4. NIR (Near infrared spectroscopy).....	6
4.2. Why NIR-spectroscopy?.....	6
4.3. FT (Fourier Transform) – IR- (Infrared) spectroscopy	7
4.4. Dispersive infrared spectroscopy.....	8
4.5. FT-IR advantages	8
4.5.1. Fast data collection	8
4.5.2. No limitation of the frequencies	8
4.5.3. Better accuracy	8
4.6. Predicting density of ribbons with NIR-spectroscopy	9
4.6.1. Diffuse reflectance	9
4.6.2. Study of predicting the density of powders with NIR-spectroscopy	10
4.6.3. First derivative	10
5. Multivariate analysis	11
5.1. PCA (principal component analysis).....	11
5.2. PLS (partial least squares).....	11
5.3. Data analysis	11
6. Experiments	12

6.1.	Materials	12
6.2.	Scale.....	13
6.3.	Bohle - BRC 25.....	13
6.4.	Experiment 01 (first experience).....	14
6.4.1.	Avicel PH 105	14
6.4.2.	Avicel PH 301	15
6.4.3.	Avicel PH 101	16
6.4.4.	Avicel PH 200	17
6.4.5.	Solka Floc	18
6.4.6.	Results of Experiment 01.....	18
6.5.	Experiment 02 (first NIR- experience).....	19
6.5.1.	Set up.....	19
6.5.2.	Process monitoring.....	20
6.5.3.	Improvement of the process monitoring model	22
6.5.4.	Results of Experiment 02.....	23
6.6.	Experiment 03 (real experiments)	24
6.6.1.	Set up.....	24
6.6.1.1.	Creation of good ribbons.....	24
6.6.1.2.	NIR-spectroscopy	25
6.6.1.3.	Determination of ribbons density.....	26
6.6.2.	Evaluation of the ribbons spectra	28
6.6.3.	Creation of PLS-models with OPUS	29
6.6.4.	Creation of PLS-models with SIMCA	30
6.6.5.	Test run to verify the PLS-models from OPUS and from SIMCA.....	31
6.6.5.1.	Test run with OPUS PLS-models.....	31
6.6.5.2.	Test run with SIMCA PLS-models	31
6.6.6.	Results of Experiment 03.....	32
6.6.6.1.	PLS-model created with OPUS for Avicel PH 102	32
6.6.6.2.	PLS-model created with SIMCA for Avicel PH 102.....	33
6.6.6.3.	Final PLS-model from OPUS for Avicel PH 102	34
6.6.6.4.	Final PLS-model from SIMCA for Avicel PH 102	35
6.6.6.5.	Score plots with SIMCA for Avicel PH 102	36

6.7. Experiment 04 (Verification of Experiment 03)	38
7. Summary	40
8. References	41

List of Figures

Figure 1: Schematic representation of the construction of a roller compactor.....	2
Figure 2: Overview of different density measurement applications in the pharmaceutical industrie ¹⁴	3
Figure 3: Ribbons from the front view, to get a more detailed view of the shape	4
Figure 4: Ribbons from the top view, to see the irregularity and to understand why calipers are useless for determination of ribbons density	4
Figure 5: Set up of the oil method to show the difference in height to determinate the density of the ribbons. a) Glass cylinder filled with oil, b) Glass cylinder filled with oil and ribbons;	4
Figure 6: GeoPyc 1360	5
Figure 7: Schematic representation of the chamber of the GeoPyc to understand how the volume is calculated. a) without sample and b) with sample. ¹⁵	5
Figure 8: Overview of different wavelength regions for a better understanding of the near infrared region of 700-2500nm ⁵	6
Figure 9: Schematic representation of an interferogram, consists of an infrared source, 2 mirrors (a stationary and a moving mirror), a beamsplitter, the sample and a detector ⁷	7
Figure 10: Development of an absorbance spectrum out of an interferogram, the intermediate step is a transmittance spectrum ⁷	7
Figure 11: Dispersive spectrometer consist of a source, sample, reference, chopper, grating, slit and detector ⁷	8
Figure 12: Difference in reflectance. a) high diffuse reflectance intensity, b) low diffuse reflectance intensity ⁸	9
Figure 13: Spectra of different compression pressures to see that the reflectance decreases with increasing pressure ⁸	9
Figure 14: Variation in calibration spectra after applying strain with the Couette cell. a) NIR spectra, b) 1st derivative of NIR calibration spectra ⁹	10
Figure 15: Formulas to calculate the RMSEP, BIAS and RSEP where n is the number of samples, y_i is the predicted value of sample i , y_i is the reference value of sample i . ¹³	11
Figure 16: Ohaus Adventurer analytical scale	13
Figure 17: Roller compactor BRC 25 from BOHLE. The main parts are: 1) feeder, 2) feeding auger, 3) tamping auger, 4) slave roller, 5) master roller, 6) milling, 7) control panel and 8) water and air pipes	13
Figure 18: Process parameters of the BRC 25, includes set points, actual values and units ...	13
Figure 19: Process control of the BRC 25 to see the actual parameter values of the production.....	13
Figure 20: Avicel PH 105, stuck inside the feeding auger due to its cohesive powder properties, necessitated manual cleaning.....	14
Figure 21: Solka Floc, stuck inside the feeding auger due to its cohesive powder properties, necessitated manual cleaning.....	18

Figure 22: Setup for collecting NIR - spectra to build the calibration model. The main set up consisted of: 1) exit of the roller compactor, 2) vibrating feeder, 3) Matrix F from Bruker and 4) dust collector.....	19
Figure 23: PLS-model for monitoring the force, green predicted values and blue reference values. For the spectra range 0-9 the force should be around 1kN, between spectrum 10-18 the force should be 5kN and a 10kN force should be for spectrum 19-27	21
Figure 24: PLS-model for monitoring the gap, green predicted values and blue reference values. For the spectra range 0-3, 3-6 and 6-9 the gap should be around 1mm, between spectrum 10-13, 13-16 and 16-19 the gap should be 2mm and a 3mm gap should be at spectrum 19-22, 22-25 and 25-28.....	21
Figure 25: Setup for the roller compactor to collect test spectra of the created ribbons to improve the existing process monitoring model and to verify that built model.	22
Figure 26: Final model for monitoring the force, green predicted values and blue reference values. Force should be around 2,5kN, which was almost the case.....	23
Figure 27: Final model for monitoring the gap, green predicted values and blue reference values. Start gap value was 1mm until spectrum 34, after that the gap was changed to 2mm. At spectrum 54 it reached steady state conditions. The last gap change to 3mm was at spectrum 115. Between spectrum 230 and 376 the gap was constant around 3mm.....	23
Figure 28: Matrix F from bruker	25
Figure 29: MicroNIR from Viavi Solutions Inc. front view	25
Figure 30: MicroNIR from Viavi Solutions Inc. top view.....	25
Figure 31: Difference in size between Matrix F and MicroNIR.....	25
Figure 32: Connection between density and force. Increasing the force increased the density. At 13kN the maximum compressibility was reached and the density did not change anymore. Trial 05 was a little bit out of the range, the reason might be wrong density determination with the GeoPyc.	27
Figure 33: Spectra from the Matrix F with OPUS. X-axis shows the wave number in cm^{-1} and the y-axis the absorbance [-]	28
Figure 34: Spectra from the Matrix F with OPUS zoomed in.....	28
Figure 35: Spectra from MicroNIR with MircoNIR Pro 2.2	28
Figure 36: Setup Quant 2 Method from Opus to create PLS-models. 3spectra of each trial were marked for test and 12 spectra for calibration. Therefore a total of 24 test and 96 calibration spectra were used.....	29
Figure 37: Simca calibration dataset. First column was marked as primary ID (yellow), second column as y-axis that contained the density (orange), and the first row was marked as secondary ID (green).	30
Figure 38: Simca test dataset. First column was marked as primary ID (yellow), second column as y-axis that contained the density (orange), and the first row was marked as secondary ID (green).	30
Figure 39: Plot/List settings. Item should be yPredPS and the y-variable the density.	30
Figure 40: Opus, Quant 2 Analysis/File List to create a test run.....	31

Figure 41: PLS-model from OPUS for Avicel PH 102 with a RMSEP of 0,072, a BIAS of 0,014 and a RSEP of 6,164%. Blue colored are the reference values from Geopyc measurements and red the predicted values. Three spectra were analyzed from each trial, and the graph thus has a total of 24 data points. The density of each trial was also determined thrice, and therefore each trial had its own reference value32

Figure 42: PLS-model from SIMCA for Avicel PH 102 within the wavelengths 1316-1496nm, with a RMSEP of 0,085, a BIAS of -0,03 and a RSEP of 7,249%. Blue colored are the reference values from Geopyc measurements and red the predicted values. Three spectra were analyzed from each trial, and the graph thus has a total of 24 data points. The density of each trial was also determined thrice, and therefore each trial had its own reference value 33

Figure 43: Final PLS-model from OPUS for Avicel PH 102 with a RMSEP of 0,061, a BIAS of 0,001 and a RSEP of 5,002%. The force was 3, 7, 9 and 13kN and the gap was constant at 1mm. Blue colored are the reference values and red the predicted values. 15 spectra were recorded from each trial, and the graph thus has a total of 60 predicted values. Three density measurements were made for each trial, therefore three reference values for each trial. ...34

Figure 44: Final PLS-model from SIMCA for Avicel PH 102 within the wavelengths 1100-1650nm, with a RMSEP of 0,179, a BIAS of -0,039 and a RSEP of 9,284%. The force was 3, 7, 9 and 13kN and the gap was 1mm. Blue colored are the reference values and red the predicted values. 15 spectra were recorded from each trial, and the graph thus has a total of 60 predicted values. Three density measurements were made for each trial, therefore three reference values for each trial.35

Figure 45: PLS-calibration score plot with SIMCA for Avicel PH 102, the ellipse describes data with a confidence interval of 95 %. In addition, you can see a trend of the density values. From left to right the density increases. Also marked with the colors blue, green yellow and orange, with a value of 0.6, 1, 1.4 and 1.536

Figure 46: PLS-score plot with SIMCA for Avicel PH 102, red = values of the calibration model, blue = predicted values. Prediction set follows the values of calibration model, therefore these models show reproducible prediction.36

Figure 47: SIMCA plot of the regression line of the prediction set (blue) and the values from the calibration set (red) for Avicel PH 102 between the wavelengths 1496 and 1650nm, the closer the points are to the straight line, the more accurate are the predicted values. On the line, prediction is equal to the observed values.37

Figure 48: PLS-model for Prosolv with a RMSEP of 0,138, a BIAS of -0,025 and a RSEP of 11,156%. Compared to the RSEP of 6,164% from the PLS-model for Avicel PH 102 this RSEP was a little bit high but still it was a good result. The reason for the high RSEP was the inaccurate density values.38

Figure 49: Final PLS-model for Prosolv with a RMSEP of 0,189, a BIAS of -0,095 and a RSEP of 14,901%. The reason for the increased RSEP was that the density value of trial 07 was incorrect. To get a better model the wrong value could be replaced. In addition, some other densities were inaccurate and can also be replaced in the future.39

List of Tables

Table 1: Overview of all tested machine parameters with Avicel PH 301	15
Table 2: Overview of all tested machine parameters with Avicel PH 101	16
Table 3: Overview of all tested machine parameters for Avicel PH 200.....	17
Table 4: Parameters for Process monitoring with Avicel PH 301	20
Table 5: Spectra for improvement of the existing process monitoring model and for verification of that built model.	22
Table 6: Parameters to create good ribbons for Avicel PH 102.....	24
Table 7: Avicel PH 102, densities of the ribbons to create the PLS-model	26
Table 8: Avicel PH 102, densities of the ribbons to verify the PLS-model	26
Table 9: Mean of densities to get an idea how the density changes with increasing the force	27
Table 10: Trials parameters to verify the PLS-models.....	31
Table 11: Data analysis of the PLS-model from OPUS.....	32
Table 12: Data analysis of the PLS-model from SIMCA	33
Table 13: Data analysis of model 4.....	34
Table 14: Data analysis of each trial.....	34
Table 15: Data analysis of the PLS-model in range 1100-1650.....	35
Table 16: Data analysis of each trial for the SIMCA model	35
Table 17: Data analysis of each trial for the PLS model for Prosolv without optimization of the density values.....	39
Table 18: Data analysis of each trial for the PLS model for Prosolv with optimization of the density values.....	39

1. Introduction

In the pharmaceutical industry where powders are used, problems such as poor flowability, segregation and lot of dust occur. Granulation processes change powder properties by agglomeration and prevent or reduce aforementioned problems. Especially dry granulation becomes more and more important, since no heat and solvent is used. Hence, it is perfect for pharmaceutical powders that are heat or moisture sensitive. Roller compaction, which is mainly used for dry granulation has different machine parameters that can be changed. Roller speed, roller gap, compaction force and the flowrate influence has been shown to most impact process performance¹. In previous studies different models were built to predict the output variables without running the roller compactor. For example there are modeling methods like finite element method, artificial neural networks models or Johanson's model. There are issues with all that existing models. The finite element method for example cannot be used for online process control or optimization¹. Models built with artificial neural networks are inherently limited by its poor extrapolation ability¹. Semi empirical models like Johanson's models are more useful, but also cannot serve the control purpose. This was decisive for the creation of a dynamic model, based on the Johanson's rolling theory and the material balance. It was one of the first models which included the dynamic behavior of the roller compactor like the roller gap, roller speed and compaction force. The main problem with that model is the interaction between input and output variables¹.

The focus of this thesis is on the density of the ribbons, since the ribbon density has been shown to be a key predictor of granule properties. Ribbons are created as an intermediate step in a roller compactor. The reason for omitting the milling part in this study is that this part would bring at least two more variables, which would make the predictive exercise very complex. In addition, the milling part is fairly well understood and the powder density can easily be predicted if the ribbon density is known.

In chapter 2 the theoretical background of the roller compactor is given. Chapter 3 focuses on different measurements for ribbon density. Near infrared spectroscopy is the topic of chapter 4 and in chapter 5 multivariate analysis is explained. Chapter 6 is dedicated to the experimental study. The summary of the thesis can be found in chapter 7 followed by references.

2. Roller Compactor

Roller compaction is a dry granulation process in the pharmaceutical area. The main goals are to improve powder properties like density and porosity for a better flowability and to prevent or reduce segregation and dust. The roller compactor process (see Figure 1) consists of following production steps: After starting the machine, the powder stored in a hopper (1), goes down into a horizontal screw, called feeding auger (2). This screw moves the powder to the tamping auger (3), a vertical screw, which pressures the powder down to the rollers. There is a rotating slave roller (4), can also be moved horizontally and a stationary rotating master roller (5). The rotation of the rollers, force the powder through them and create ribbons as a byproduct. These ribbons get into a rotating sieve which acts like a mill (6) and breaks the ribbons to powder again.

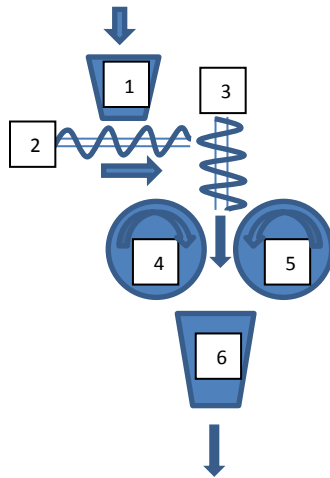


Figure 1: Schematic representation of the construction of a roller compactor

The behavior of the roller compactor process is mainly dependent on the roller speed, roller gap and compaction force. In addition, the process can be influenced by the speed of the feeding auger or by the dosing percentage (ratio between feeding and tamping auger).

3. Density of roller compacted ribbons

In this chapter, different types of densities were discussed, followed by 3 methods, which were used in this thesis to ascertain ribbons density.

3.1. Overview of different densities

At first sight, one can imagine that the volume of a solid body can be easily determined only by measuring the length, width and height. On closer examination, however, it is noticeable that most of the solids consist of structural irregularities, fissures and pores, which affect the volume, whether they are visible on the surface or are only in the interior of the material. Therefore, different existing volumes can be measured, hence different densities².

For example:

True density: Density of a solid without all pores, can be performed on APIs, excipients, blends and tablets³

Apparent density: Nearly the same as true density, except the closed pores volume is also included. If the true density of powder is different to true density of the tablet, the volume of the closed pores can be determined³.

Bulk density: Additionally to the volume of the material it includes all pores and the holes between the particles. Describes the volume of broken materials like powder, granules or grains³.

Envelope density: Almost the same as bulk density, but it is for a single, consolidated quantity of material, hence no holes between particles exist³.

An overview of different density measurement applications is given in Figure 2.

For this thesis the envelope density is the critical value, since it changes with the compaction force. Hence, it is possible to connect different machine parameter with the envelope density of roller compacted ribbons.

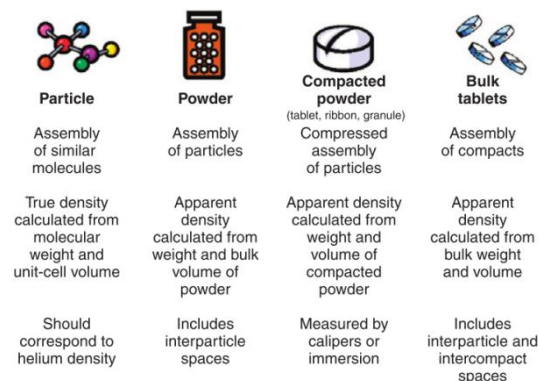


Figure 2: Overview of different density measurement applications in the pharmaceutical industrie¹⁴

3.2. Measurement of ribbon density

Density determination is challenging, especially for porous systems like roller compacted ribbons.

3.2.1. Caliper

In order to determine the density of ribbon, it is necessary to know the mass and the volume of the ribbon. The mass can easily be obtained through a scale. For the volume the first try was to measure the length, breadth and height with a caliper. For regular shaped ribbons it was a good method. The ribbons got from the roller compactor BRC 25, which was used in this thesis, created irregular ribbons. Hence, calipers are useless for this purpose (Figure 3 and Figure 4).

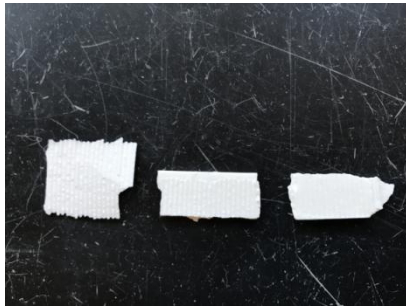


Figure 3: Ribbons from the top view, to see the irregularity and to understand why calipers are useless for determination of ribbons density



Figure 4: Ribbons from the front view, to get a more detailed view of the shape

3.2.2. Oil method

This method is based on the increase of the fluid volume inside a cylinder. Oil, was filled into a glass cylinder and served as a measuring fluid (see Figure 5a). The filling height was then noted down and a few ribbons were weighed and dropped into it (see Figure 5b). When the ribbons were totally on the cylinder bottom and only a few bubbles were left, the fluid height was read again. Out of the difference in height and the diameter of the glass cylinder, the volume of the ribbons was calculated (see Figure 5a, and Figure 5b). The main problems were that the increase in height was not easy to visualize. There were always some bubbles left and the oil got into the pores of the ribbons. This resulted in inaccurate measurements of density.

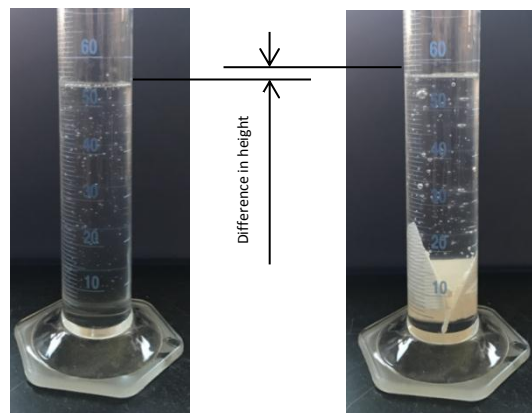


Figure 5: Set up of the oil method to show the difference in height to determinate the density of the ribbons. a) Glass cylinder filled with oil, b) Glass cylinder filled with oil and ribbons;

3.2.3. GeoPyc

In this thesis the GeoPyc 1360 was used (see Figure 6). It is a density measurement technique that uses a fluid called DryFlo, which consist of small rigid spheres that have a high degree of flowability. DryFlo covers the sample surface totally, since it has a small particle size. The chamber where the fluid is placed is a precision bore glass cylinder. There are different chamber sizes available: 12,7mm, 19,1mm, 25,4mm, 38,1mm and 50,8mm⁴. For each chamber size different forces and conversion factors are necessary.

For the ribbons the chamber needed to be a bigger one, so 38,1mm was chosen. Before the first measurement, a zero depth calibration test must be performed for each chamber in order to determine the exact depth of the cylinder. Then, the chamber was filled with DryFlo, the typical consolidation force was set at 90 kN, the conversion factor was set at 1,1492 cm³/mm, the cycle number for both runs was set at 7 (Only DryFlo resp. DryFlo and sample) and the sample weight was entered. The plunger compressed the DryFlo until the force of 90kN was reached. The length from the DryFlo to the plunger was measured and set as baseline A (see Figure 7a). When this distance was twice quite the same the countdown of 7 cycles started. When the blank run was finished, the sample was added to the DryFlo and the procedure was restarted. Again the force was 90kN. The run with the sample had a different distance called baseline B, since the volume has increased (see Figure 7b). This displacement in baselines gave the distance h. With this value, the volume of the sample was calculated as $v=r^2*\pi*h$. At the end the sample volume, envelope density and its standard deviation were on the display of the GeoPyc.



Figure 6: GeoPyc 1360

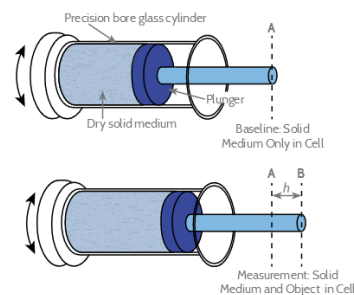


Figure 7: Schematic representation of the chamber of the GeoPyc to understand how the volume is calculated. a) without sample and b) with sample.¹⁵

4. NIR (Near infrared spectroscopy)

Near infrared spectroscopy occurs in the wavelength range 700-2500nm (see Figure 8)⁵. In this NIR-region the absorption bands mainly correspond to overtones and vibrations⁶. The focus of this thesis is on the physical aspects, so no further discussion is made on chemical principles.

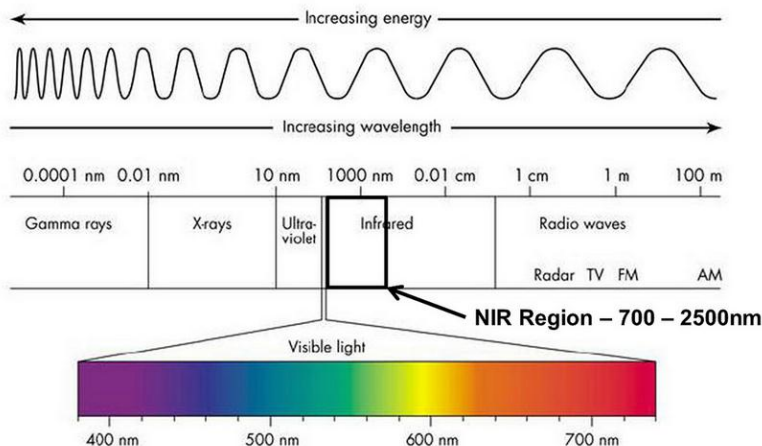


Figure 8: Overview of different wavelength regions for a better understanding of the near infrared region of 700-2500nm⁵

4.2. Why NIR-spectroscopy?

In recent years NIR spectroscopy has become more and more important in the pharmaceutical industries. The main reasons for this growth compared to other analytical techniques are its advantages like:

- No pretreatment of samples
- No impairment or destruction of the samples
- Less time-consuming
- Real time measurement
- Near infrared models can be constructed by using reference values from traditional measurements and obtain faster results

Furthermore, calibration models by near infrared spectroscopy for tablets had been constructed for similar properties, such as compaction force, hardness and dissolution.

4.3. FT (Fourier Transform) - IR- (Infrared) spectroscopy

The main part of a FT-Instrument is a system called interferometer. It consists of a beamsplitter which separates the beam into two parts. One section is then transmitted to mirror which moves constantly with the same velocity. The rest of the beam is reflected to a stationary mirror. Both beams recombine again at the beamsplitter, after they have been reflected from the mirrors. At the same time interference pattern, called an interferogram, is created, since some of the wavelengths have recombined destructively⁷.

In the next step some energy of the interferogram is transmitted and some is absorbed from the sample. Only the transmitted part reaches the detector, where the information about every wavelength is read simultaneously⁷ (see Figure 9).

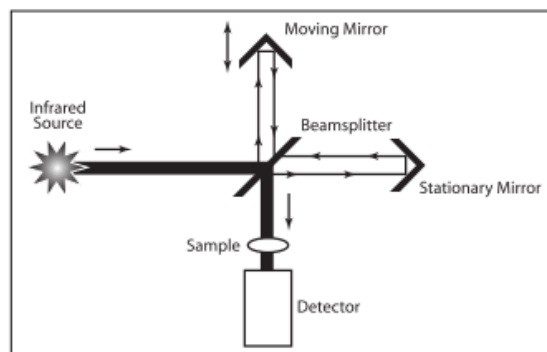


Figure 9: Schematic representation of an interferogram, consists of an infrared source, 2 mirrors (a stationary and a moving mirror), a beamsplitter, the sample and a detector⁷

This information is then sent to a computer, where an algorithm called Fourier Transformation is performed. It converts the interferogram into a single beam spectrum. In order to make this happen first a background single beam spectrum must be recorded and divided by return value of the sample single beam spectrum. The result of this procedure is the transmittance spectrum in percentage. To obtain the absorbance spectrum out of the transmittance spectrum, the negative \log_{10} of the data points is necessary⁷ (see Figure 10).

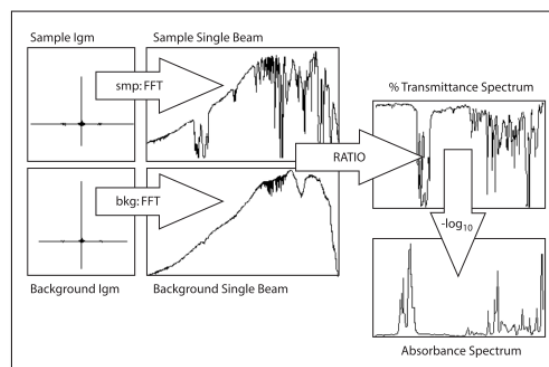


Figure 10: Development of an absorbance spectrum out of an interferogram, the intermediate step is a transmittance spectrum⁷

4.4. Dispersive infrared spectroscopy

In a dispersive infrared spectrometer a mirror divides the beam which comes from a source into two parts. One beam goes through the sample and the second one goes through the reference. After that both beams go through the chopper, which moderates the energy, and then to the grating. The grating, similar to a prism, separates the wavelengths of light and moves each wavelength individually through a slit to the detector. The grating and a slit assembly allows the selection of the wavelength being measured.⁷ (see Figure 11).

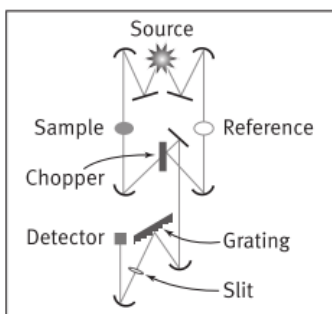


Figure 11: Dispersive spectrometer consist of a source, sample, reference, chopper, grating, slit and detector⁷

4.5. FT-IR advantages

Compared to the dispersive spectrometer the FT-IR spectrometer has three major advantages. Fast data collection, no limitation of the frequencies and better accuracy. Hence, nowadays FT-IR spectrometers are getting more popular⁷.

4.5.1. Fast data collection

The FT-IR spectrometer can measure the entire spectra range very fast, since the interferometer inside doesn't separate the energy in different frequencies. Furthermore individual scans can be combined to give better results. The dispersive spectrometer takes much longer, since every wavelength needs to be measured individually⁷.

4.5.2. No limitation of the frequencies

The slit in a dispersive infrared spectrometer limits the energy that goes through the sample and enters the detector; hence the signal-to-noise ratio of the infrared spectra is lower than in a FT-IR spectrometer. That means in a FT-IR spectrometer the sensitivity of small peaks will be greater, therefore the details in a spectrum will be clearer visible. In addition, there are less reflection losses compared to the dispersive infrared spectrometer⁷.

4.5.3. Better accuracy

For spectra collected with a FT-IR; the time of recording doesn't matter, since the laser wavelength is a constant value and these points are automatically referenced to the x-axis data points of the FT-IR spectrum. In dispersive infrared spectrometers external calibration values are required, which make the results less comparable and the process less accurate⁷.

4.6. Predicting density of ribbons with NIR-spectroscopy

This chapter gives information about the theoretical background of predicting density with NIR-spectroscopy. First diffuse reflectance is explained, followed by a study of predicting density of powders with NIR-spectroscopy and the first derivative method.

4.6.1. Diffuse reflectance

In order to predict the density of ribbons with NIR spectroscopy it is necessary to understand the relationship between compression pressure and diffuse reflectance. In high compressed materials particles are closer to each other than in less packed materials, because of that they are transmitting much more light⁸ (see Figure 12).

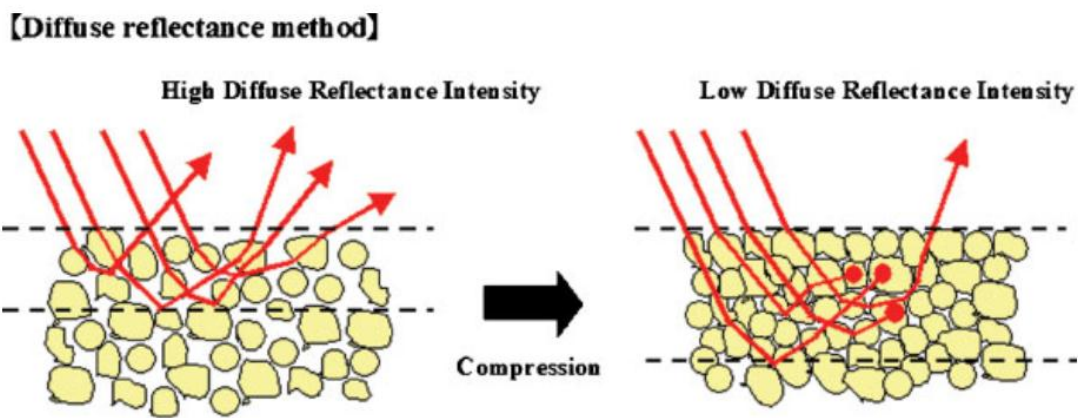


Figure 12: Difference in reflectance. a) high diffuse reflectance intensity, b) low diffuse reflectance intensity⁸

The phenomena described above can also be seen in the spectra of the NIR spectroscopy. For higher compression pressures the reflectance decreases, because of that you can see that the baseline in the spectra also decreases⁸ (see Figure 13).

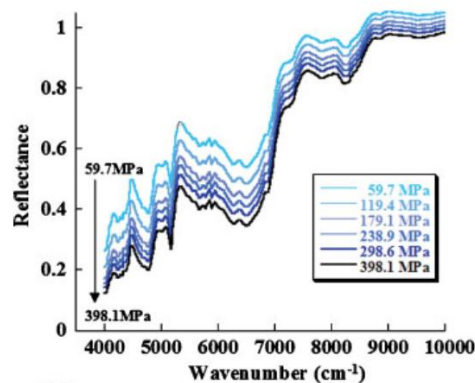


Figure 13: Spectra of different compression pressures to see that the reflectance decreases with increasing pressure⁸

4.6.2. Study of predicting the density of powders with NIR-spectroscopy

Based on the knowledge discussed above an exploratory study was performed to evaluate the possibility of using NIR-spectrometers to measure density of porous materials. A FT4 powder rheometer was used to obtain different density levels of a powder bed. In this case, a compressibility test produced a normal force which acted on the powder and created packed powder. Of each sample, compressed at different compression forces, a NIR-spectrum was recorded. For increasing density the baseline also increased, which indicated that less radiation reached the detector (reflectance decreases). The results of this study confirmed that high packed particles lead to less diffuse radiation as the transmitted radiation increased. However, it was observed that the shift in baseline changed even with the same conditions; hence the result was not reproducible. Since this cannot be used for predicting density of powders, another method needed to be found.⁹

4.6.3. First derivative

The method employed for predicting density of powders with NIR-spectroscopy was the use of first derivative of the spectra. The first derivative eliminated the shift in baseline, while the differences in spectral slope were clarified. Each spectrum had different slopes, which changed with the density of the powders, enabling quantification and subsequently prediction of powders with different densities.⁹ Figure 14 shows the plot of the calibration spectra and the first derivative of these spectra.

Based on the success of the first derivative for powders, it was decided to use this method for predicting density of roller compacted ribbons.

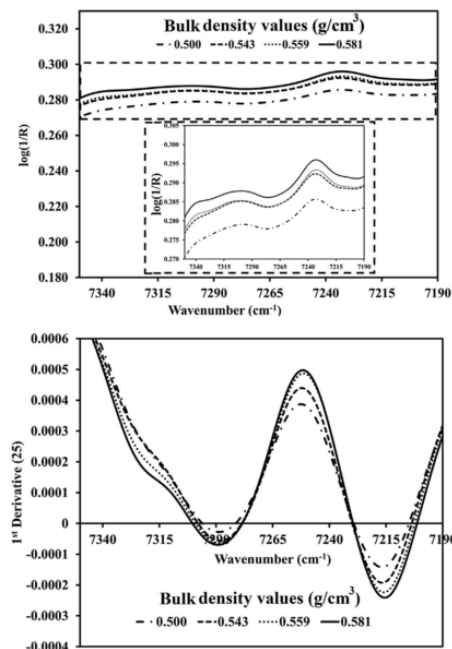


Figure 14: Variation in calibration spectra after applying strain with the Couette cell. a) NIR spectra, b) 1st derivative of NIR calibration spectra⁹.

5. Multivariate analysis

Multivariate analysis means evaluation of data with a minimum of six variables to millions. This chapter gives an overview of two mainly used methods to analyze this data, namely PCA and PLS method¹⁰.

5.1. PCA (principal component analysis)

This method uses inter-correlated quantitative dependent variables to describe observations from a data table. To extract the important information out of this table and to show this in a new set of variables, called principal components, are its main goals. In addition, the similarity between observations and new variables is shown. Different validation techniques are required to evaluate these PCA models.¹¹

5.2. PLS (partial least squares)

Compared to PCA modeling, which is based on the underlying correlation among variables only, the PLS methods explicitly exposes the existence of causal relationships.¹²

5.3. Data analysis

The performance of the PLS-models was evaluated with 3 values, namely the RMSEP (Root Mean Square Error of Prediction), BIAS and the RSEP (Relative Standard Error of Prediction in %). The exact formulas to calculate those values are shown in Figure 15. However, the most important value was the RSEP, since it gives an idea how accurate the model is.¹³

$$RMSEP = \sqrt{\frac{\sum_{i=1}^n (\hat{y}_i - y_i)^2}{n}}$$
$$BIAS = \frac{1}{n} \sum_{i=1}^n (\hat{y}_i - y_i)^2$$
$$RSEP = \sqrt{\frac{\sum_{i=1}^m (\hat{y}_i - y_i)^2}{\sum_{i=1}^m y_i^2}} * 100\%$$

Figure 15: Formulas to calculate the RMSEP, BIAS and RSEP where n is the number of samples, \hat{y}_i is the predicted value of sample i , y_i is the reference value of sample i .^{9,13}

6. Experiments

In this chapter, we first look at the various materials that were used, afterwards the equipment used is shown and finally the actual experimental results are examined in more detail. The experiments consist of three sub-areas. The first attempts which were necessary to become familiar with the roller compactor and to find out how the machine can be used are summarized in Experiment 01. Experiment 02 is about initial tests with NIR spectrometers. All knowledge is then collated in Experiment 03, where a model was constructed to predict the density of roller compacted ribbons. Finally the Experiment 04 was made to verify if the Experiment 03 is useful for other materials.

6.1. Materials

Microcrystalline Cellulose, NF, Ph. Eur., JP (MCC)

FMC Biopolymer, Philadelphia, PA

- Avicel PH 101, median particle size 50 µm
- Avicel PH 102, median particle size 100 µm
- Avicel PH 105, median particle size 20 µm,
- Avicel PH 200, median particle size 180 µm
- Avicel PH 301, median particle size 50 µm

Powdered Cellulose

International Fiber Corporation Urbana, Ohio

- Solka Floc,

Silicified Microcrystalline Cellulose

(Composed of Microcrystalline Cellulose, NF, Ph. Eur., JP & Colloidal Silicon Dioxide, NF, Ph. Eur., JP)

JRS Pharma GmbH & Co. KG, Rosenberg, Germany

- Prosolv SMCC HD 90

6.2. Scale

In order to get the density of the ribbons, the volume and also the mass are needed. For mass measurement the Adventurer analytical scale from OHAUS was used (see Figure 16). This scale is very accurate, since it can be totally closed. In addition, the horizontal adjustable feet always ensure a straight working surface. The ribbons were put on weighing boats for exact measurements. To get good results a high samples weight is needed, hence in our case 5 ribbons were weighed together.

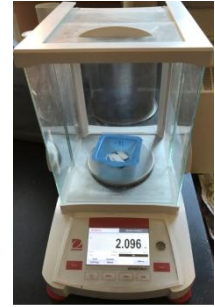


Figure 16: Ohaus Adventurer analytical scale

6.3. Bohle - BRC 25

In chapter 2, the scheme of a roller compactor is given. In this chapter the roller compactor BRC 25 from BOHLE, shown in Figure 17, is described. In addition to the same 6 parts already shown in chapter 2, the BRC 25 consists of a control panel (7), water and air pipe (8) for cleaning. In our case, the connection was not built; hence no automatic cleaning was possible. For safety reasons, the BRC25 has many sensors. For example, the machine can only be started when the door is closed, the outlet is in position, and the sensor touches a surface inside the hopper (so there must be enough material inside). The process parameters can be directly changed and monitored through the control panel (see Figure 18 and Figure 19).

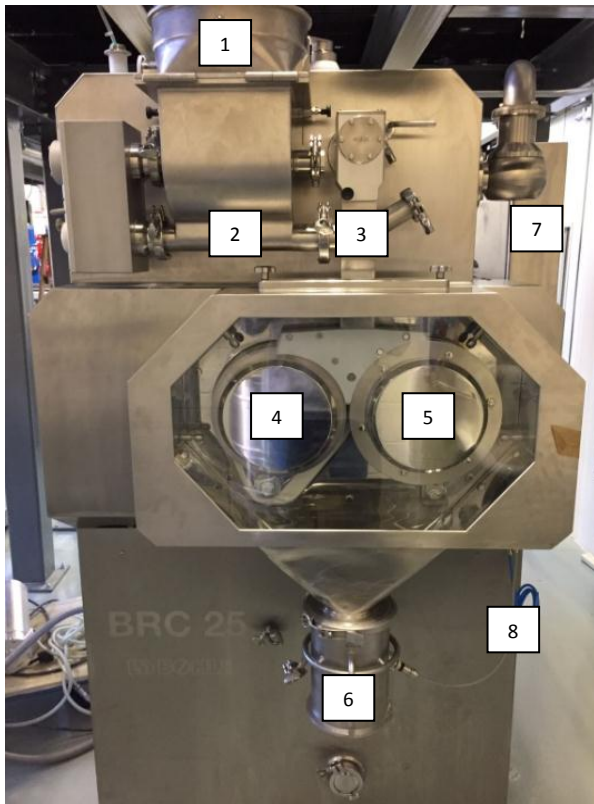


Figure 17: Roller compactor BRC 25 from BOHLE. The main parts are: 1) feeder, 2) feeding auger, 3) tamping auger, 4) slave roller, 5) master roller, 6) milling, 7) control panel and 8) water and air pipes

Parameter	Set point	Act. value	Unit
Duration of production	99	15	min
Dosing			
Dosing relation: tamping-, feeding auger	100	100	%
Speed feeding auger	66.4	66.4	rpm
Speed tamping auger	209.1	209.0	rpm
Compact			
Speed master roller	10.0	10.0	rpm
Speed slave roller	10.0	10.0	rpm
Spec. compact force	2.5	2.5	kN/cm
Roller gap	3.0	3.0	mm
Sieve			
Speed sieve	400	400	rpm

Figure 18: Process parameters of the BRC 25, includes set points, actual values and units

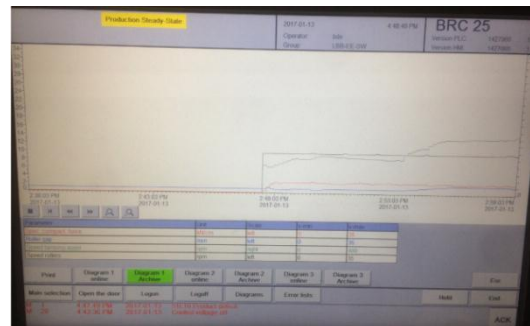


Figure 19: Process control of the BRC 25 to see the actual parameter values of the production

6.4. Experiment 01 (first experience)

The goal of this experiment is getting experience with the roller compactor and finding out the machine parameters range to get good ribbons. Only machine parameters like force, gap, roller speed and dosing percentage were changed. This experiment was performed with different Avicel grades (PH 105, PH 301, PH 101 and PH 200) and Solka Floc.

6.4.1. Avicel PH 105

Since Avicel PH 105 is the Avicel grade with the smallest particle size and most compressible one, good ribbons were expected, hence it was the first material tested with the BRC 25. This material stuck inside the feeding auger after 25min, due to its cohesive powder properties, and necessitated manual cleaning (see Figure 20). Hence, no further experiments were performed with Avicel PH 105.



Figure 20: Avicel PH 105, stuck inside the feeding auger due to its cohesive powder properties, necessitated manual cleaning

6.4.2. Avicel PH 301




This experiment gives an overview of different machine settings (see Table 1). The following parameters have been changed:

Force: 1, 5 (only trial 00), 10 and 20 kN

Gap: 1, 3 and 6 mm

Roller Speed: 5, 10, 20 and 30 rpm

A total of 37 trials were performed (3 forces*3 gaps*4 roller speeds + Trial 00).

 good ribbons  much powder  parameter didn't work

Dosing % = Relation between feeding auger and tamping auger

Table 1: Overview of all tested machine parameters with Avicel PH 301

Trial Nr. [-]	Force [kN]	Roller Gap [mm]	Roller Speed [rpm]	Dosing %/ Speed tamping auger	Trial Nr. [-]	Force [kN]	Roller Gap [mm]	Roller Speed [rpm]	Dosing %/ Speed tamping auger
00	5	1	5	600/120,7	19	1	1	20	200/388,9
01	1	1	5	200/42,6	20	1	2,8	20	200/388,9
02	1	3	5	600/209,5	21	1	6	20	200/388,9
03	1	6	5	200/300	22	10	1	20	100/388,9
04	10	1	5	200/202,2	23	10	3	20	
05	10	3	5	200/358,9	24	10	6	20	
06	10	3,5	5	100/388,9	25	20	1	20	
07	20	1	5		26	20	3	20	
08	20	3	5		27	20	6	20	
09	20	6	5		28	1	1	30	100/196
10	1	1	10	200/103	29	1	3	30	200/388,9
11	1	3	10	200/291	30	1	6	30	200/388,9
12	1	6	10	100/388,9	31	10	1	30	200/388,9
13	10	1	10	200/198	32	10	3	30	200/198
14	10	2,5	10	100/388,9	33	10	6	30	200/388,9
15	10	6	10		34	20	1	30	200/388,9
16	20	1	10		35	20	3	30	200/388,9
17	20	3	10		36	20	6	30	200/388,9
18	20	6	10						

6.4.3. Avicel PH 101

Only those parameters which showed positive results for Avicel PH 301 were tested in this case. A total of 9 trials out of 12 were tested, because there was no material left for the last 3 runs (Table 2). All the tested parameters showed nearly the same behavior as they did with material PH 301.

good ribbons
 much powder
 short of material

Dosing % = Relation between feeding auger and tamping auger

Table 2: Overview of all tested machine parameters with Avicel PH 101

Trial Nr. [-] C	Force [kN]	Roller Gap [mm]	Roller Speed [rpm]	Dosing % Speed tamping auger
00	5	1	5	600/229
01	1	1	5	250/85,3
02	1	3	5	600/300
04	10	1	5	200/165
05	10	3	5	200/314
10	1	1	10	200/388,9
11	1	3	10	200/291
13	10	1	10	
19	1	1	20	200/254
20	1	3	20	
22	10	1	20	
28	1	1	30	100/196

6.4.4. Avicel PH 200

Since the particle size of PH 301 and PH 101 is the same, PH 200 should provide further validation if the parameter range determined above is suitable for all Avicel grades. For this test the same machine settings were used as that for Avicel PH 301 (Table 3).

Force: 1, 5 (only trial 00), 10 and 20 kN

Gap: 1, 3 and 6 mm

Roller Speed: 5, 10, 20 and 30 rpm

A total of 37 trials were performed (3 forces*3 gaps*4 roller speeds + Trial 00).

 good ribbons  much powder  didn't work

Dosing % = Relation between feeding auger and tamping auger

Table 3: Overview of all tested machine parameters for Avicel PH 200

Trial Nr. [-]	Force [kN]	Roller Gap [mm]	Roller Speed [rpm]	Dosing %/ Speed tamping auger	Trial Nr. [-]	Force [kN]	Roller Gap [mm]	Roller Speed [rpm]	Dosing %/ Speed tamping auger
00	5	1	5	200/80,7	19	1	1	20	200/186
01	1	1	5	200/65	20	1	3	20	100/388,9
02	1	3	5	600/181,7	21	1	6	20	200/388,9
03	1	6	5	200/300	22	10	1	20	100/376
04	10	1	5	100/98,7	23	10	3	20	
05	10	3	5	200/358,9	24	10	6	20	
06	10	6	5	100/388,9	25	20	1	20	
07	20	1	5		26	20	3	20	
08	20	3	5		27	20	6	20	
09	20	6	5		28	1	1	30	150/227,4
10	1	1	10	200/103	29	1	3	30	200/388,9
11	1	3	10	200/219,5	30	1	6	30	200/388,9
12	1	6	10	100/388,9	31	10	1	30	100/388,9
13	10	1	10	200/210	32	10	3	30	
14	10	2,5	10	100/388,9	33	10	6	30	
15	10	6	10		34	20	1	30	
16	20	1	10		35	20	3	30	
17	20	3	10		36	20	6	30	
18	20	6	10						

6.4.5. Solka Floc

Solka Floc also stuck inside the feeding auger after 25min, due to its cohesive powder properties and the shape of its primary particles. That necessitated manual cleaning (Figure 21).



Figure 21: Solka Floc, stuck inside the feeding auger due to its cohesive powder properties, necessitated manual cleaning

6.4.6. Results of Experiment 01

The Experiment 01 showed that not all powders were useable in the BRC 25. Pure Avicel PH 105 and Solka Floc tended to stick inside the feeding auger. In addition, the tests gave a good overview of the parameter working space. The force of 20kN and the gap of 6mm were not possible with the BRC 25 for Avicel PH 301, PH 101 and PH 200. The roller speed changed mainly the flow rate and least affected the properties of the ribbons. Even at the maximum roller speed of 30rpm it was possible to produce ribbons, but only at a low gap or force. If the gap or the force was increased beyond a certain threshold, the machine failed to reach the desired set points and the production shut down. Of all useable settings, at which ribbons were produced, they were optically analyzed. To get good ribbons the gap should be around 1 mm and the force should not be higher than 15kN, since the powder over compresses, which results in fragile ribbons.

6.5. Experiment 02 (first NIR- experience)

In order to predict density of roller compacted ribbons some pretests, like Experiment 01 and Experiment 02 needed to be performed. This section discusses finding the best setup for further tests, gives an idea about different machine settings, and introduces the NIR- spectrometers and the concept of creating chemo metric models.

6.5.1. Set up

Roller compacted ribbons came through the BRC25 exit (1) into the vibrating feeder (2). The surface of the feeder should be completely covered with ribbons, since the measuring range of NIR - spectrometer (3) is equal to width of the channel. For this experiment, the Matrix F from Bruker was used. The thickness of the ribbon layers was adjusted by the vibrations intensity of the feeder. The vibratory feeder emptied into a collection bucket. This setup produced a lot of dust and hence a portable dust collector (4) was used (as shown in Figure 22).

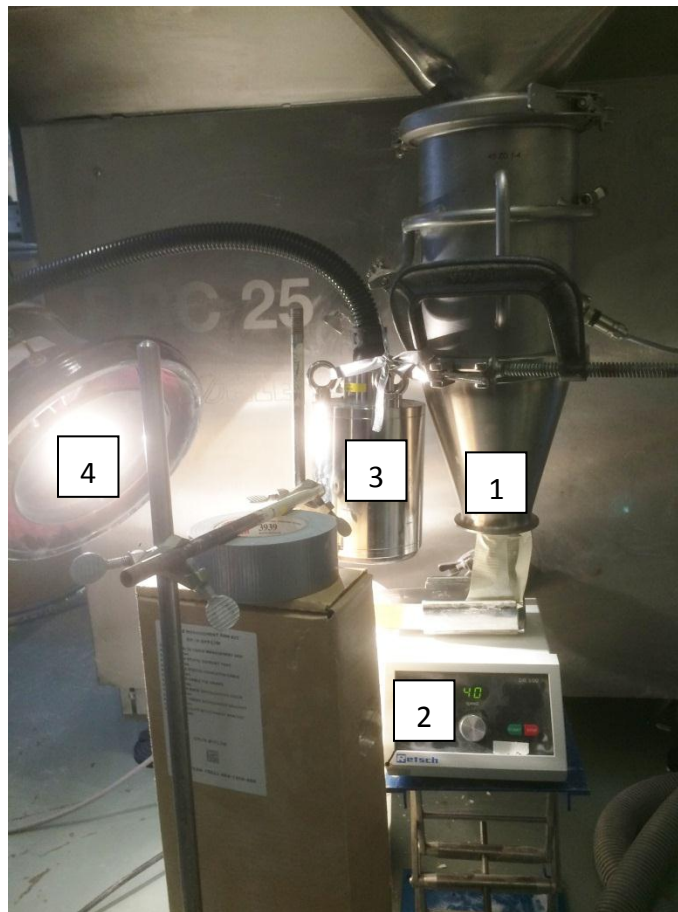


Figure 22: Setup for collecting NIR - spectra to build the calibration model. The main set up consisted of: 1) exit of the roller compactor, 2) vibrating feeder, 3) Matrix F from Bruker and 4) dust collector

6.5.2. Process monitoring

In this chapter the development of PLS-models, with the Software 7.5 from OPUS is shown. These models were created for a quick overview about the possibilities and limitations of the NIR-spectroscopy. Only first derivatives were considered, because this method attenuates the shift of the baseline and highlights the spectral slope⁹.

To obtain a good model for process monitoring, it is necessary to choose a useful range of machine parameters. The experiment 01 showed which parameters mainly affect the process and how they can be adjusted in order to achieve good results. The experiment 01 also showed that the roller gap should not be too high, and therefore the roll gaps used for this test were 1, 2 and 3 mm. Compression force of 1, 5 and 10 kN were used and the roller speed was kept constant at 10rpm. A total of 9 trials (3 different gaps * 3 different forces * 1 roller speed = 9trials) were considered for this model (Table 4).

Table 4: Parameters for Process monitoring with Avicel PH 301

Trial Nr. [-]	Force [kN]	Gap [mm]	Roller Speed [rpm]	Dosing %/ Speed tamping auger
1	1	1	10	100/106,7
2	1	2	10	150/166,2
3	1	3	10	100/193,3
4	5	1	10	100/134
5	5	2	10	100/227
6	5	3	10	100/335
7	10	1	10	260/323,3
8	10	2	10	150/347,7
9	10	3	10	100/388,9

NIR-spectra of ribbons from all trials were used to build the chemometric models with OPUS. 40 spectra of each trial were recorded and analyzed. Out of that, the best 33 spectra were used. 30 of each trial were used to create a process monitoring model. Finally 2 models for process monitoring were developed. The remaining 3 spectra of each trial were used to perform a test run.

Only the compression force was changed in the first test run. The actual force values should follow the set parameters (1kN, 5kN and 10kN) in the spectra range (0-9, 10-18, 19-27). This behavior could be seen in Figure 23; hence monitoring the force was possible with this method.

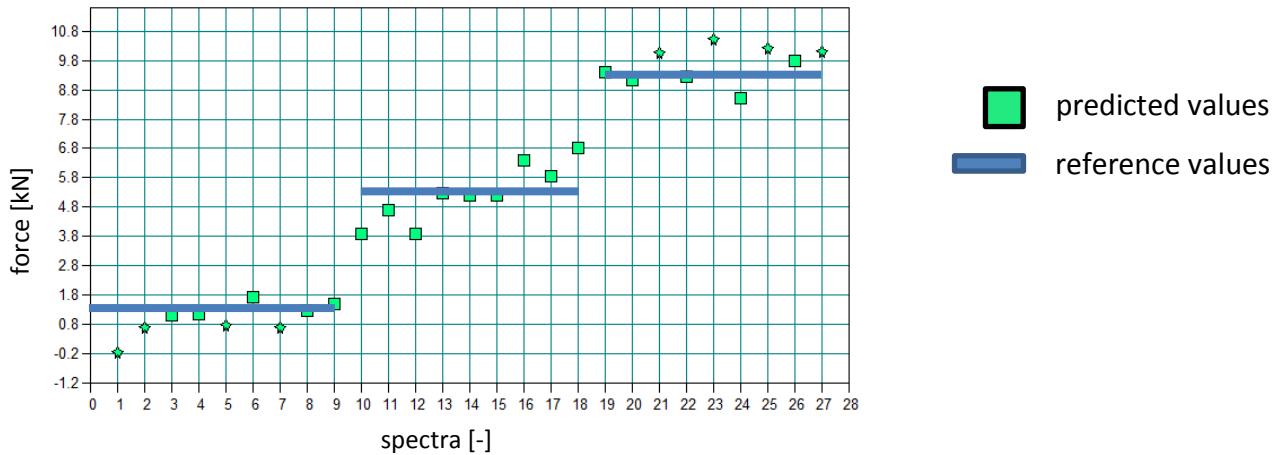


Figure 23: PLS-model for monitoring the force, green predicted values and blue reference values. For the spectra range 0-9 the force should be around 1kN, between spectrum 10-18 the force should be 5kN and a 10kN force should be for spectrum 19-27

The second model intended to predict the roller gap. In this case, the actual gap values should follow the set parameters (1mm, 2mm and 3mm) in the spectra range (0-3, 3-6, 6-9 the same for 10-13, 13-16, 16-19 and for 19-22, 22-25, 25-28). As can be seen in Figure 24, the model predictions were fairly inaccurate, due to insufficient number of total available spectra.

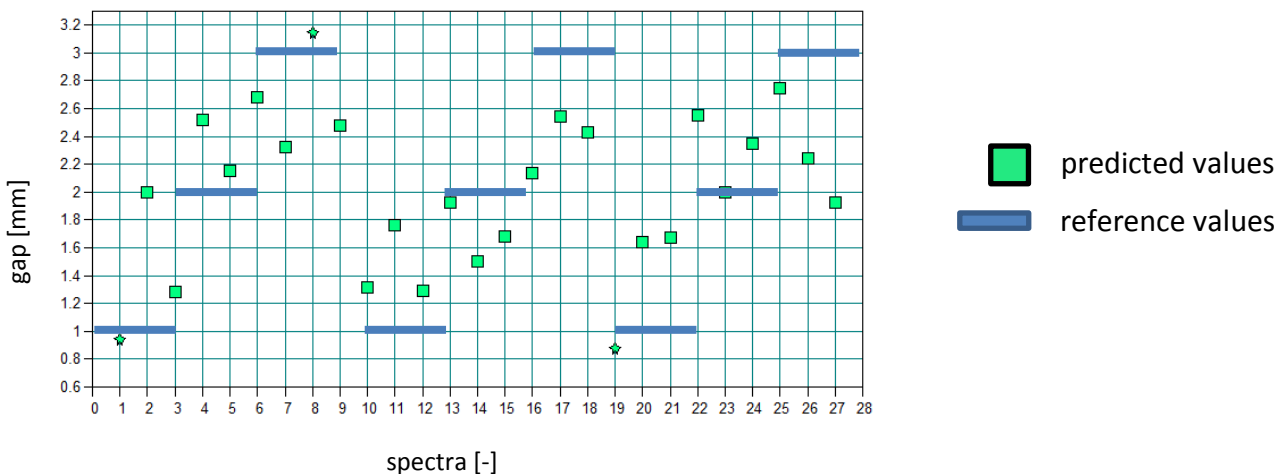


Figure 24: PLS-model for monitoring the gap, green predicted values and blue reference values. For the spectra range 0-3, 3-6 and 6-9 the gap should be around 1mm, between spectrum 10-13, 13-16 and 16-19 the gap should be 2mm and a 3mm gap should be at spectrum 19-22, 22-25 and 25-28

6.5.3. Improvement of the process monitoring model

To improve the first models some new spectra were collected. The setup was almost the same as in section 6.5.1 (see Figure 25); suction was used as well, but is not in the picture. For these spectra the force was always 2,5kN and the roller speed was kept constant at 10 rpm. The gap changed between 1, 2 and 3 mm. Spectra were continuously recorded with the NIR- Matrix F every 3 seconds. A total of 377 test spectra were recorded and evaluated (see Table 5). The best spectra were then added to the old dataset and a new model was built. The remaining new spectra were then used to test the veracity of the new model.

Table 5: Spectra for improvement of the existing process monitoring model and for verification of that built model.

Trial Nr. [-]	Force [kN]	Gap [mm]	Roller Speed [rpm]	Spectra-Nr. [-]
1	2,5	1	10	0-37
2	2,5	2	10	54-115
3	2,5	3	10	230-376



Figure 25: Setup for the roller compactor to collect test spectra of the created ribbons to improve the existing process monitoring model and to verify that built model.

6.5.4. Results of Experiment 02

The results of experiment 02 showed that it is possible to monitor the process of the roller compactor via NIR-spectroscopy. The actual values of the force were around 2,5kN, which means that this is a good result for further tests with the NIR-spectrometer (see Figure 26).

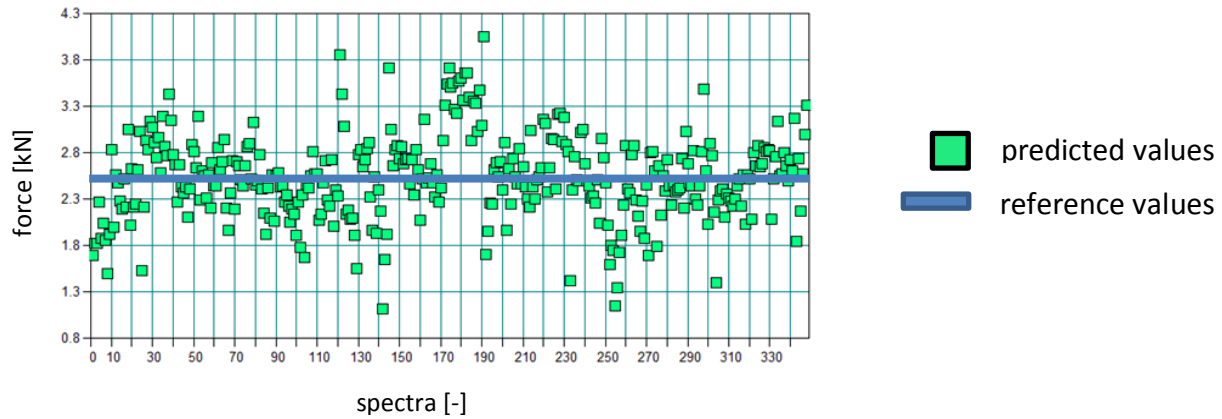


Figure 26: Final model for monitoring the force, green predicted values and blue reference values. Force should be around 2,5kN, which was almost the case.

The same procedure was used for monitoring the roller gap. In the first 34 spectra the actual value follows 1mm, after which the gap was set to 2mm. At spectrum 54 the gap was constantly 2mm, and the predicted value also showed the same behavior. The last gap step, to 3mm, was made at spectrum 115. It took until spectrum number 230 to reach steady state conditions. The whole process can be seen in Figure 27. All in all, the predicted gap value was always around the set gap value; hence NIR-spectroscopy might be useful for predicting the roller gap as well. The ability to successfully predict roll pressure and roller gap lends itself to successful prediction of ribbon density.

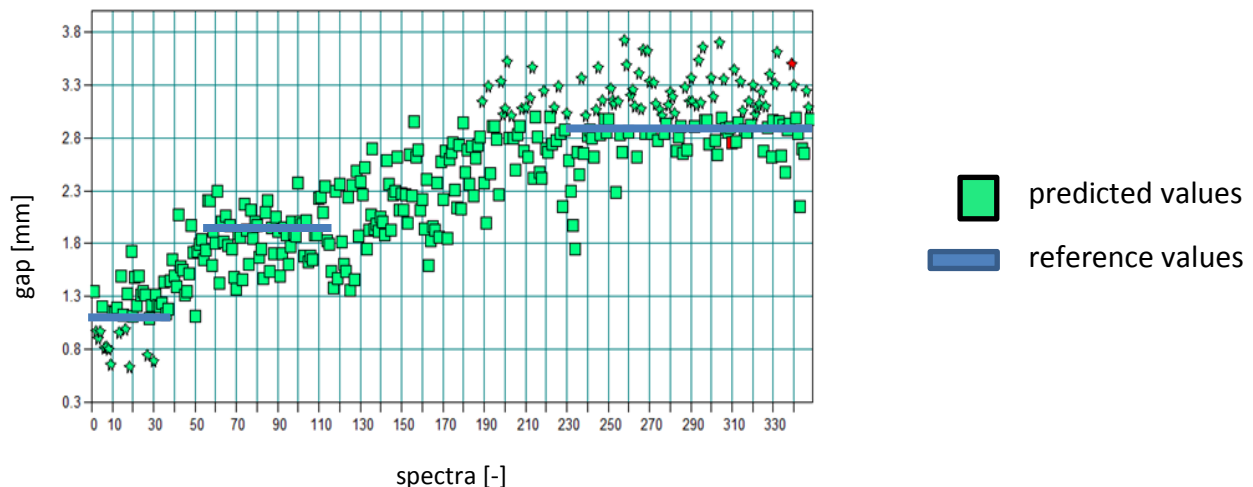


Figure 27: Final model for monitoring the gap, green predicted values and blue reference values. Start gap value was 1mm until spectrum 34, after that the gap was changed to 2mm. At spectrum 54 it reached steady state conditions. The last gap change to 3mm was at spectrum 115. Between spectrum 230 and 376 the gap was constant around 3mm.

6.6. Experiment 03 (real experiments)

In this chapter, the experiences of previous experiments are compiled to predict the density of roller compacted ribbons. The material used is Avicel PH 102. The aim is to collect ribbons under different conditions, to acquire spectra with NIR spectrometers, to measure the mass with a scale and to determine the density with the Geopyc and to combine these values to create a PLS model. The first step was making this procedure offline with the Matrix F from Bruker. The MicroNIR was also used because it fits into the roller compactor and can therefore be used inline. The reason the MicroNIR was also used offline, was to find out whether it is as accurate as Bruker's Matrix F because it is a dispersive infrared spectrometer (see section 4.4) and to find out if inline measurements can be done outside of its working distance. Normally, this distance should be about 3 mm, for the BRC 25 the minimum possible distance was about 1.5 cm.

6.6.1. Set up

To make this possible, many things had to be considered. First, it was necessary to create good ribbons under different conditions. Furthermore, it was important that the NIR spectrometer and the density determination with the GeoPyc were accurate enough. The last significant step was to build usable PLS models.

6.6.1.1. Creation of good ribbons

This time the ribbons were collected directly after the exit of the roller compactor, since the spectra were recorded separately. The Experiment 01 showed the gap should be around 1mm to create good ribbons; therefore the gap was set at 1mm. In addition, the previous experiments showed low influence of the roller speed, because of that the speed was set to 10rpm and the dosing percentage was set to 200. Hence the force was the only variable parameter. A step of 2kN was chosen, with a start value of 1kN. The maximum reachable force was 16kN; therefore 15kN was the maximum for this experiment. So at 8 different force steps, ribbons were created and collected (shown in Table 6).

Table 6: Parameters to create good ribbons for Avicel PH 102

Trial Nr. [-]	Force [kN]	Gap [mm]	Roller Speed [rpm]	Dosing %/ Speed tamping auger
0	1	1	10	200/28,8
1	3	1	10	200/40,7
2	5	1	10	200/49,1
3	7	1	10	200/51,1
4	9	1	10	200/55,5
5	11	1	10	200/59
6	13	1	10	200/66,4
7	15	1	10	200/69,9

6.6.1.2. NIR-spectroscopy

As already mentioned, the Bruker Matrix F and the MicroNIR from Viavi Solutions Inc. were used to collect NIR spectra (see Figure 28 and Figure 29). The difference of these two NIR spectrometers is described in chapter 4 and shown in Figure 31. In order to guarantee good results, 5 ribbons were laid side by side and another ribbon was placed on their surface. The reason for the second series was that when the NIR went between 2 ribbons, it did not hit another surface. This operation was performed three times, so 30 ribbons were required for each trial. The spectra from only the top ribbons; were recorded. All together there were 15 spectra of each experiment and NIR-spectrometer (see in Figure 30).

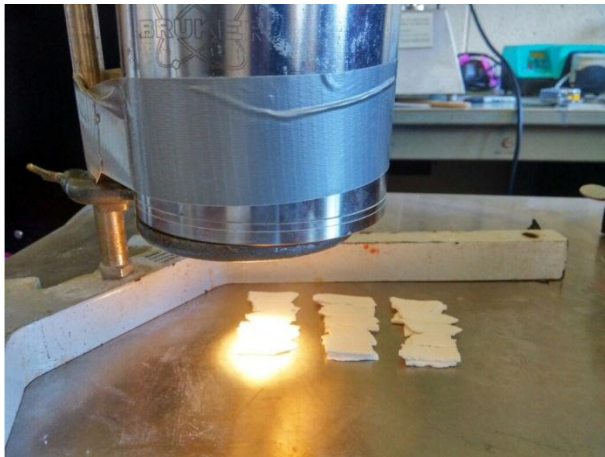


Figure 28: Matrix F from Bruker



Figure 29: MicroNIR from Viavi Solutions Inc. front view



Figure 30: MicroNIR from Viavi Solutions Inc. top view

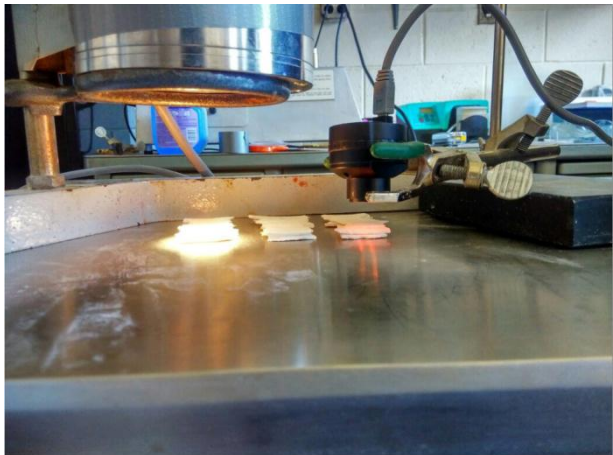


Figure 31: Difference in size between Matrix F and MicroNIR

6.6.1.3. Determination of ribbons density

As already discussed in chapter 3, determination of ribbons density was a challenge. With the GeoPyc described in section 3.2.3, it was possible to obtain the ribbons density. We found that a sample quantity of 5 ribbons and a layer of 2cm DryFlo lead to good results. The optimum ratio between DryFlo and sample volume is 2/3. 5 ribbons were used for each run, resulting in 3 density measurements per trial. This was also the reason to make the set up described in chapter 6.6.1. Only fresh DryFlo was used, since the experience showed that polluted DryFlo can influence the results. The density measurements were performed in triplicate (see Table 7 and Table 8). Some of the results were out of range; attributed to a wrong ratio between sample and DryFlo.

Table 7: Avicel PH 102, densities of the ribbons to create the PLS-model

trial Nr. [-]	Mass [g]	Density [g/cm ³]	std. deviation [g/cm ³]
00	1,88	0,759	0,004
	1,723	0,7879	0,022
	1,776	0,8052	0,0053
01	2,567	0,9515	0,0026
	2,068	0,7904	0,0015
	2,692	0,9428	0,0023
02	3,051	1,002	0,0023
	2,969	1,1352	0,0038
	2,716	1,0668	0,0037
03	3,457	1,1903	0,0008
	2,954	1,1691	0,0015
	2,967	1,2316	0,0046
04	3,754	1,2953	0,005
	3,585	1,3182	0,0018
	3,652	1,1425	0,0013
05	3,72	1,3075	0,003
	3,964	1,2026	0,0053
	4,577	1,1759	0,0162
06	4,562	1,2959	0,0015
	4,505	1,3858	0,002
	3,886	1,4264	0,0055
07	4,546	1,3474	0,002
	4,219	1,4523	0,0016
	3,207	1,371	0,0065

Table 8: Avicel PH 102, densities of the ribbons to verify the PLS-model

trial Nr. [-]	Mass [g]	Density [g/cm ³]	std. deviation [g/cm ³]
01	2,536	0,9892	0,0009
	2,382	0,9401	0,0039
	2,302	0,935	0,009
03	4,211	1,1766	0,0059
	3,76	1,1656	0,0029
	4,437	1,1773	0,0023
04	4,08	1,3102	0,0035
	3,792	1,3002	0,0068
	3,21	1,4347	0,011
06	3,822	1,3426	0,004
	3,3	1,3352	0,0039
	3,148	1,3937	0,0107

For a better overview of the relation between force and density, the behavior is shown in Figure 32. To achieve this, the mean value of the densities was calculated (Table 9). Beyond a force of 13kN, the maximum compressibility was reached and the force no longer affected the density. The density always increased with increasing force, except in the case of trial 05. In trial 05, a mistake was made with the density measurement. All other tests showed good results.

Table 9: Mean of densities to get an idea how the density changes with increasing the force

trial Nr. [-]	force [kN]	Density [g/cm ³]
00	1	0,784
01	3	0,895
02	5	1,068
03	7	1,197
04	9	1,252
05	11	1,229
06	13	1,369
07	15	1,390

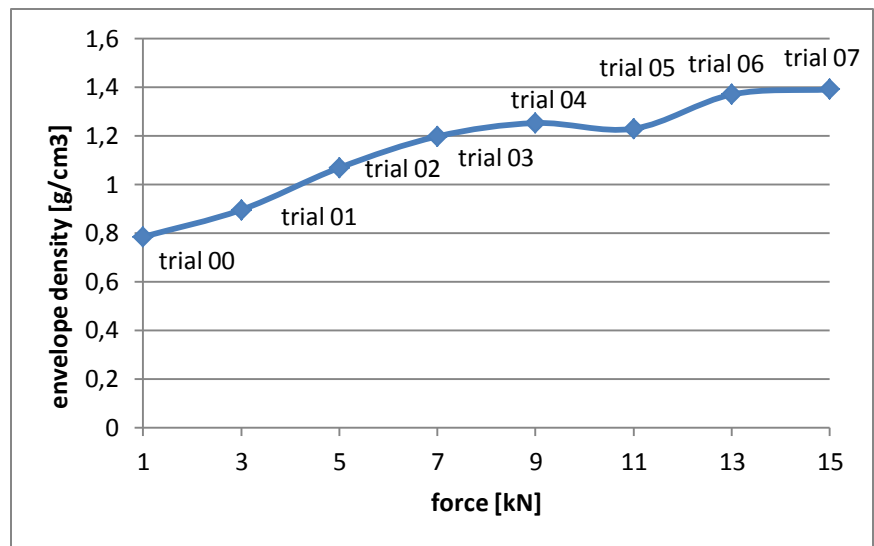


Figure 32: Connection between density and force. Increasing the force increased the density. At 13kN the maximum compressibility was reached and the density did not change anymore. Trial 05 was a little bit out of the range, the reason might be wrong density determination with the GeoPyc.

6.6.2. Evaluation of the ribbons spectra

For acquisition of spectra from the Bruker Matrix F, the software OPUS was used, see Figure 33 and Figure 34, and the MicroNIR Pro 2.2 software was used to collect the MicroNIR spectra, see Figure 35. In order to compare both spectra visually, the OPUS spectrum was zoomed in, because it had the unit cm^{-1} and the MicroNIR spectra the unit nanometer (Figure 34 and Figure 35). However, the spectra of both spectrometers were treated separately from each other for the prediction of the density of ribbons, so no conversion of the units was necessary.

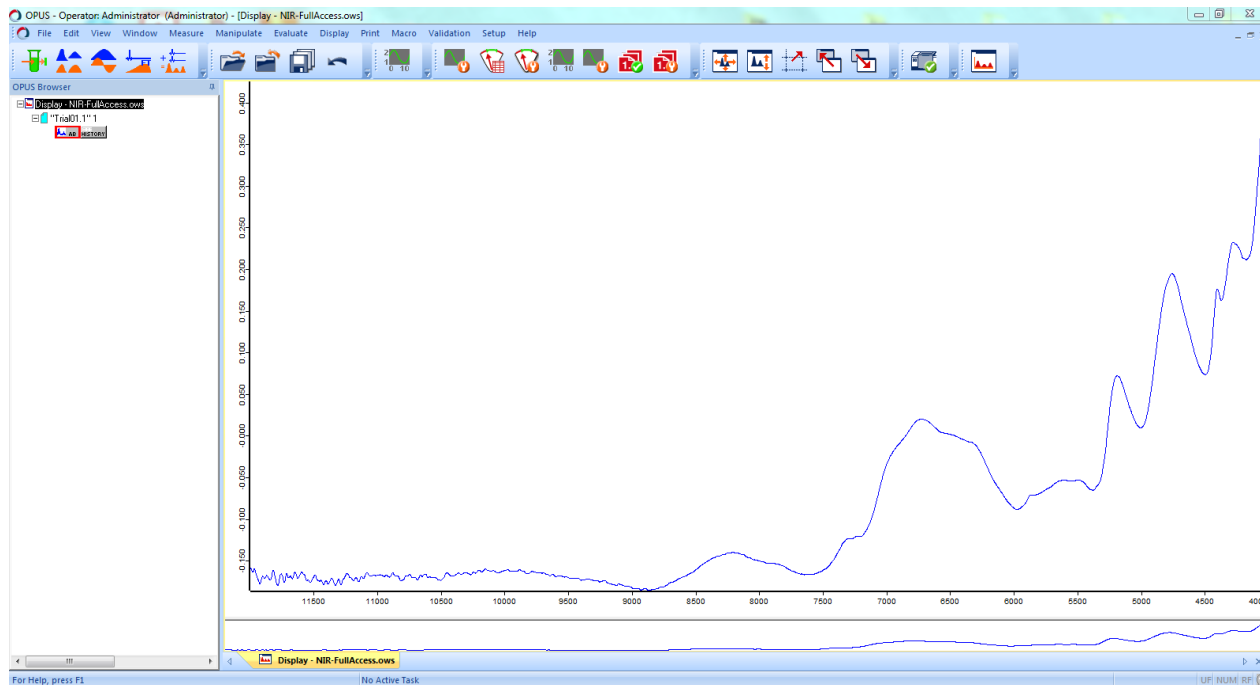


Figure 33: Spectra from the Matrix F with OPUS. X-axis shows the wave number in cm^{-1} and the y-axis the absorbance [-]

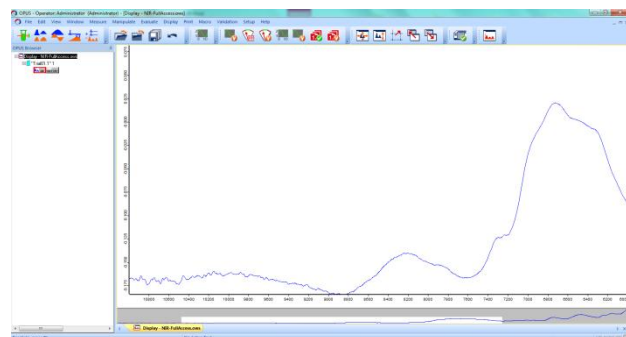


Figure 34: Spectra from the Matrix F with OPUS zoomed in

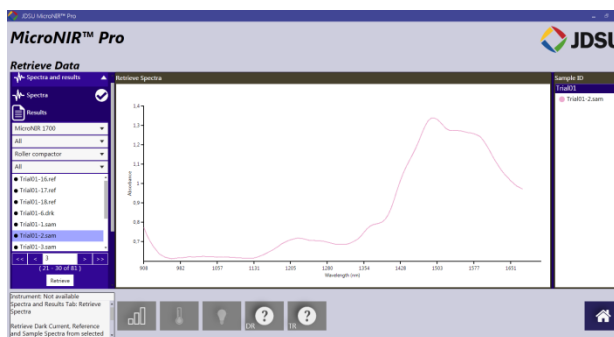


Figure 35: Spectra from MicroNIR with MicroNIR Pro 2.2

6.6.3. Creation of PLS-models with OPUS

In order to gain methods for density prediction, the menu "Setup Quant 2 Method" from OPUS was used. First in the sub-point "components" density in g/cm^3 was entered, followed by the spectra. From each trial, the first spectra of each 5 series were marked as test and all others were marked as calibration (see Figure 36). Therefore, there were 24 test and 96 calibration spectra. All these values have then been connected with the actual density value obtained from GeoPyc. After that, the test validation was done and finally optimized. Only first derivatives were considered (see section 4.6). Out of 45 first derivative models, only four models with the lowest RMSEP were taken and analyzed further.

	Data Set	Sample	Path	File Name	density
1	Test	1	C:\Users\Luk	Trial0 (1).0	0.759
2	Calibration	1	C:\Users\Luk	Trial0 (1).1	0.759
3	Calibration	1	C:\Users\Luk	Trial0 (1).2	0.759
4	Calibration	1	C:\Users\Luk	Trial0 (1).3	0.759
5	Calibration	1	C:\Users\Luk	Trial0 (1).4	0.759
6	Test	2	C:\Users\Luk	Trial0 (2).0	0.7879
7	Calibration	2	C:\Users\Luk	Trial0 (2).1	0.7879
8	Calibration	2	C:\Users\Luk	Trial0 (2).2	0.7879
9	Calibration	2	C:\Users\Luk	Trial0 (2).3	0.7879
10	Calibration	2	C:\Users\Luk	Trial0 (2).4	0.7879
11	Test	3	C:\Users\Luk	Trial0 (3).0	0.8052
12	Calibration	3	C:\Users\Luk	Trial0 (3).1	0.8052
13	Calibration	3	C:\Users\Luk	Trial0 (3).2	0.8052
14	Calibration	3	C:\Users\Luk	Trial0 (3).3	0.8052
15	Calibration	3	C:\Users\Luk	Trial0 (3).4	0.8052
16	Test	4	C:\Users\Luk	Trial01 (1).0	0.9515
17	Calibration	4	C:\Users\Luk	Trial01 (1).1	0.9515
18	Calibration	4	C:\Users\Luk	Trial01 (1).2	0.9515
19	Calibration	4	C:\Users\Luk	Trial01 (1).3	0.9515
20	Calibration	4	C:\Users\Luk	Trial01 (1).4	0.9515

Figure 36: Setup Quant 2 Method from Opus to create PLS-models. 3spectra of each trial were marked for test and 12 spectra for calibration. Therefore a total of 24 test and 96 calibration spectra were used.

6.6.4. Creation of PLS-models with SIMCA

The software SIMCA was used to obtain the models for the density prediction from the spectra of the MicroNir. To use the SAM file created in MicroNir Pro v2.2 in SIMCA, it had to be converted to a CSV file first. The PLS models were built for different wavelengths. A separate model was constructed for the entire range, the wavelength between 1100-1650 nm, 1316-1496 nm and 1496-1650 nm. First a data set for the calibration (see Figure 37) and a dataset for the test were created (see Figure 38). For the test dataset, the values 1, 6 and 11 of each trial were used and thus removed from the calibration dataset. In both datasets, the first column was the primary ID, the second column was marked as the y axis that contained the density, and the first row was the secondary ID.

Figure 37: Simca calibration dataset. First column was marked as primary ID (yellow), second column as y-axis that contained the density (orange), and the first row was marked as secondary ID (green).

Figure 38: Simca test dataset. First column was marked as primary ID (yellow), second column as y-axis that contained the density (orange), and the first row was marked as secondary ID (green).

After that the data need to be fitted via autofit. The next step is creating a list in the sub menu of SIMCA plot/list with the same settings shown in Figure 39. Finally the predicted values are shown in a table.

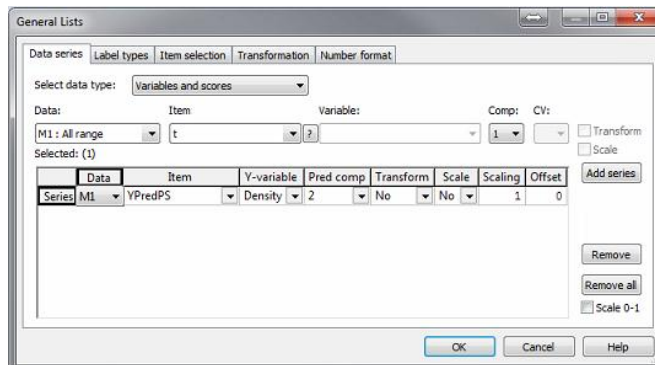


Figure 39: Plot/List settings. Item should be yPredPS and the y-variable the density.

6.6.5. Test run to verify the PLS-models from OPUS and from SIMCA

For verification of the PLS-model, the whole procedure described in section 6.6.1 was performed again for test 1, 3, 4 and 6 (see Table 10). These trials were chosen, because they cover the entire sample area.

Table 10: Trials parameters to verify the PLS-models

Trial Nr. [-]	Force [kN]	Gap [mm]	Roller Speed [rpm]	Dosing %/ Speed tamping auger
1	3	1	10	200/40,7
3	7	1	10	200/51,1
4	9	1	10	200/55,5
6	13	1	10	200/66,4

6.6.5.1. Test run with OPUS PLS-models

To verify the PLS-models from OPUS, the menu "Quant 2 Analysis/File List" was used. First the PLS-models obtained from the procedure of section 6.6.3 were added to the methods, secondly the new spectra were added and finally the results were analyzed (see Figure 40).

File Name	Sample Name	Method	Component	Prediction	Unit	Outside	Mah. Dist.
1	Trial01.0 batch 1	1.q2	density	1.0557	g/cm³	0.0022	(
2	Trial01.1 batch 1	1.q2	density	1.0423	g/cm³	0.0035	(
3	Trial01.2 batch 1	1.q2	density	1.0469	g/cm³	0.0035	(
4	Trial01.3 batch 1	1.q2	density	1.043	g/cm³	0.0033	(
5	Trial01.4 batch 1	1.q2	density	1.002	g/cm³	0.0076	(
6	Trial01.5 batch 1	1.q2	density	1.0461	g/cm³	0.0033	(
7	Trial01.6 batch 1	1.q2	density	1.0426	g/cm³	0.0034	(
8	Trial01.7 batch 1	1.q2	density	1.0271	g/cm³	0.0047	(
9	Trial01.8 batch 1	1.q2	density	1.0052	g/cm³	0.0061	(
10	Trial01.9 batch 1	1.q2	density	1.0459	g/cm³	0.0033	(
11	Trial01.10 batch 1	1.q2	density	1.062	g/cm³	0.0024	(
12	Trial01.11 batch 1	1.q2	density	1.0031	g/cm³	0.0063	(
13	Trial01.12 batch 1	1.q2	density	1.0495	g/cm³	0.0031	(
14	Trial01.13 batch 1	1.q2	density	1.0361	g/cm³	0.004	(
15	Trial01.14 batch 1	1.q2	density	1.009	g/cm³	0.0062	(
16	Trial03.0 batch 1	1.q2	density	1.1904	g/cm³	0.0023	(
17	Trial03.1 batch 1	1.q2	density	1.1628	g/cm³	0.0032	(
18	Trial03.2 batch 1	1.q2	density	1.1627	g/cm³	0.0019	(
19	Trial03.3 batch 1	1.q2	density	1.2049	g/cm³	0.0023	(
20	Trial03.4 batch 1	1.q2	density	1.1227	g/cm³	0.00064	(

Figure 40: Opus, Quant 2 Analysis/File List to create a test run

6.6.5.2. Test run with SIMCA PLS-models

In order to verify the PLS-model from SIMCA the new spectra were added to the dataset and a new list was made. The results were then plotted in an Excel file.

6.6.6. Results of Experiment 03

In this chapter the results of Experiment 03 are presented. The results of the PLS-models from OPUS and SIMCA are shown in an Excel graph. Finally the test runs of the PLS-models, also shown in an Excel graph, are discussed.

6.6.6.1. PLS-model created with OPUS for Avicel PH 102

For all 4 PLS-models the RMSEP, BIAS and the RSEP was calculated and evaluated (described in section 5.3). The model with the lowest relative standard error of prediction was considered as the best model. In this case it was called model 1. The predicted values follow the reference values from GeoPyc with a RMSEP of 0,072, BIAS of 0,014 and the RSEP of 6,164 % (see Figure 41 and Table 11).

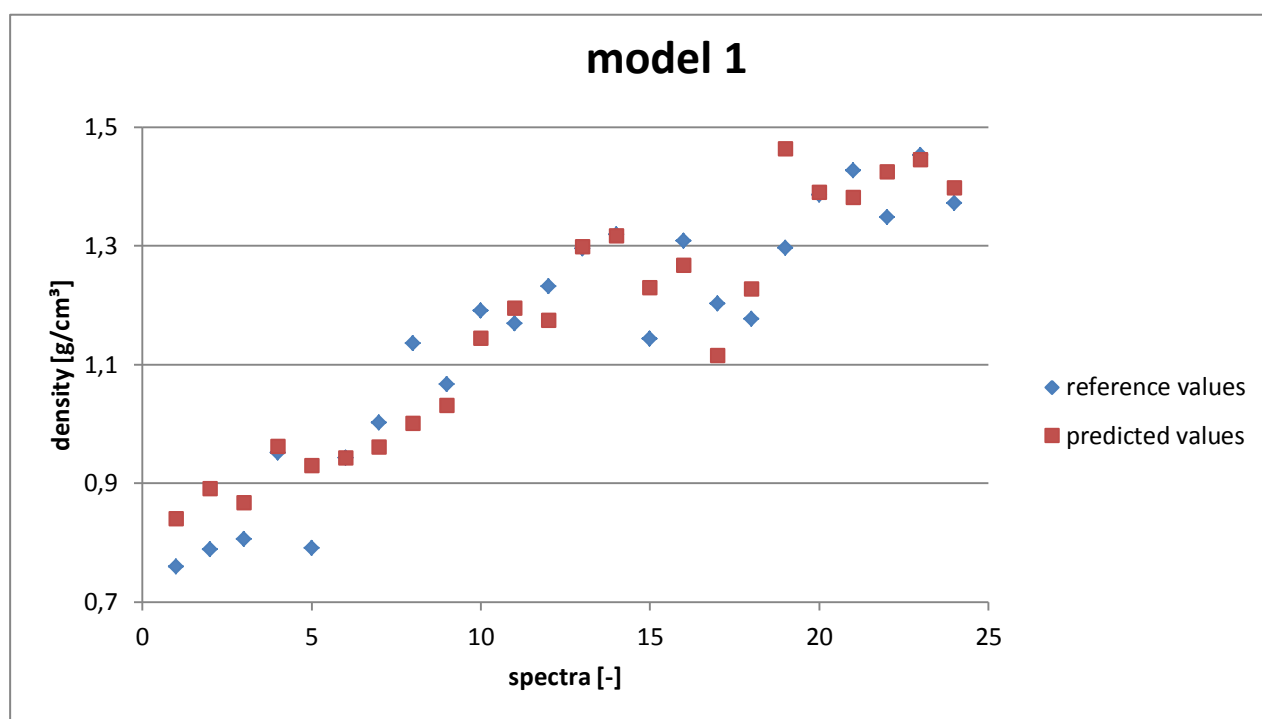


Figure 41: PLS-model from OPUS for Avicel PH 102 with a RMSEP of 0,072, a BIAS of 0,014 and a RSEP of 6,164%. Blue colored are the reference values from Geopyc measurements and red the predicted values. Three spectra were analyzed from each trial, and the graph thus has a total of 24 data points. The density of each trial was also determined thrice, and therefore each trial had its own reference value

Table 11: Data analysis of the PLS-model from OPUS

RMSEP [-]	BIAS [-]	RSEP [%]
0,072	0,014	6,164

6.6.6.2. PLS-model created with SIMCA for Avicel PH 102

The same procedure as in the section above was followed to obtain for the results from SIMCA. In the range 1316-1496 nm the best model was obtained. The predicted values follow the reference values from GeoPyc with a RMSEP of 0,085, BIAS of 0,030 and the RSEP of 7,249 (see Figure 42 and Table 12)

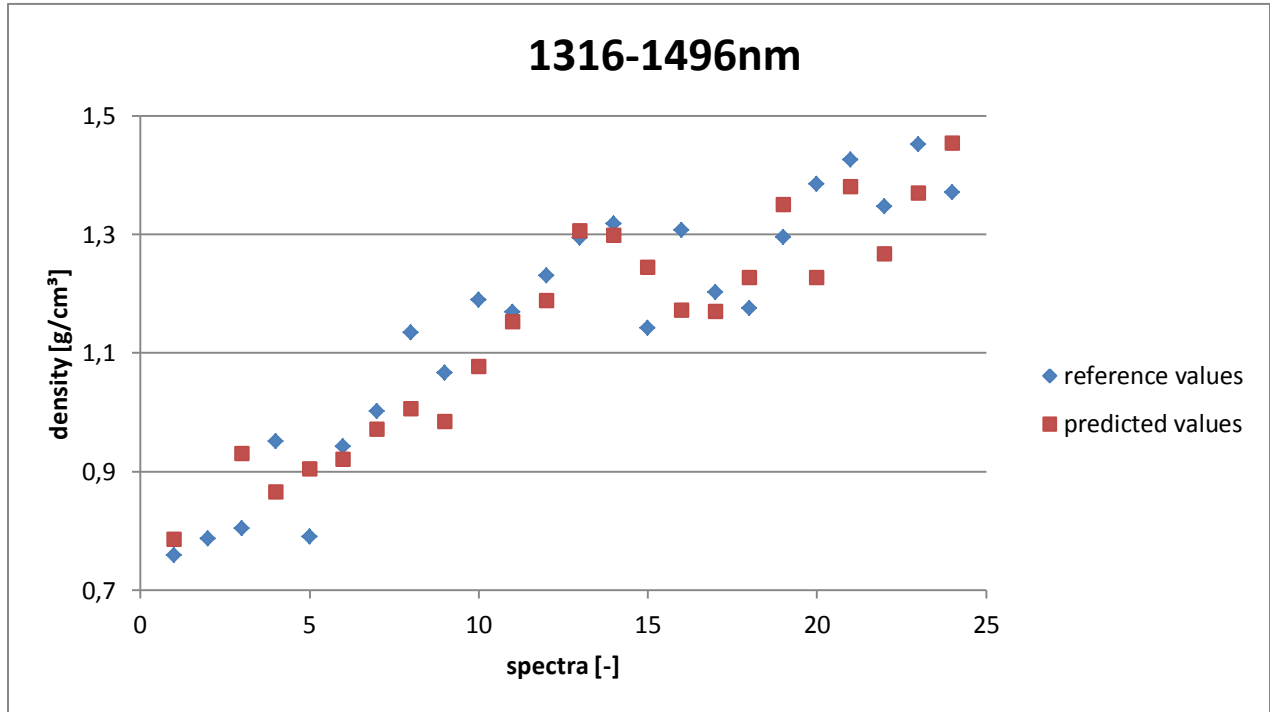


Figure 42: PLS-model from SIMCA for Avicel PH 102 within the wavelengths 1316-1496nm, with a RMSEP of 0,085, a BIAS of -0,03 and a RSEP of 7,249%. Blue colored are the reference values from Geopyc measurements and red the predicted values. Three spectra were analyzed from each trial, and the graph thus has a total of 24 data points. The density of each trial was also determined thrice, and therefore each trial had its own reference value

Table 12: Data analysis of the PLS-model from SIMCA

RMSEP [-]	BIAS [-]	RSEP [%]
0,085	-0,03	7,249

6.6.6.3. Final PLS-model from OPUS for Avicel PH 102

From the 4 verification PLS models, Model 4 was the best because it had a RSEP of 5,002 which was the lowest of all models (see Figure 43 and Table 13). Therefore, this model also showed how much the predicted values follow the actual values. The RSEP was then calculated for each different density step, since Model 4 showed that in some experiments the predicted values are closer to the reference values than in other trials. The calculations confirmed this behavior. Trial 7 had the lowest RSEP with 3.754%, which means that the predicted values are very close to the actual values. For trial 01 the RSEP was the highest with 6,136% (see Table 14). The reason for different RSEPs may be that the GeoPyc is more accurate for ribbons with a higher density because the material is no longer compressible, hence there is less fluctuation.

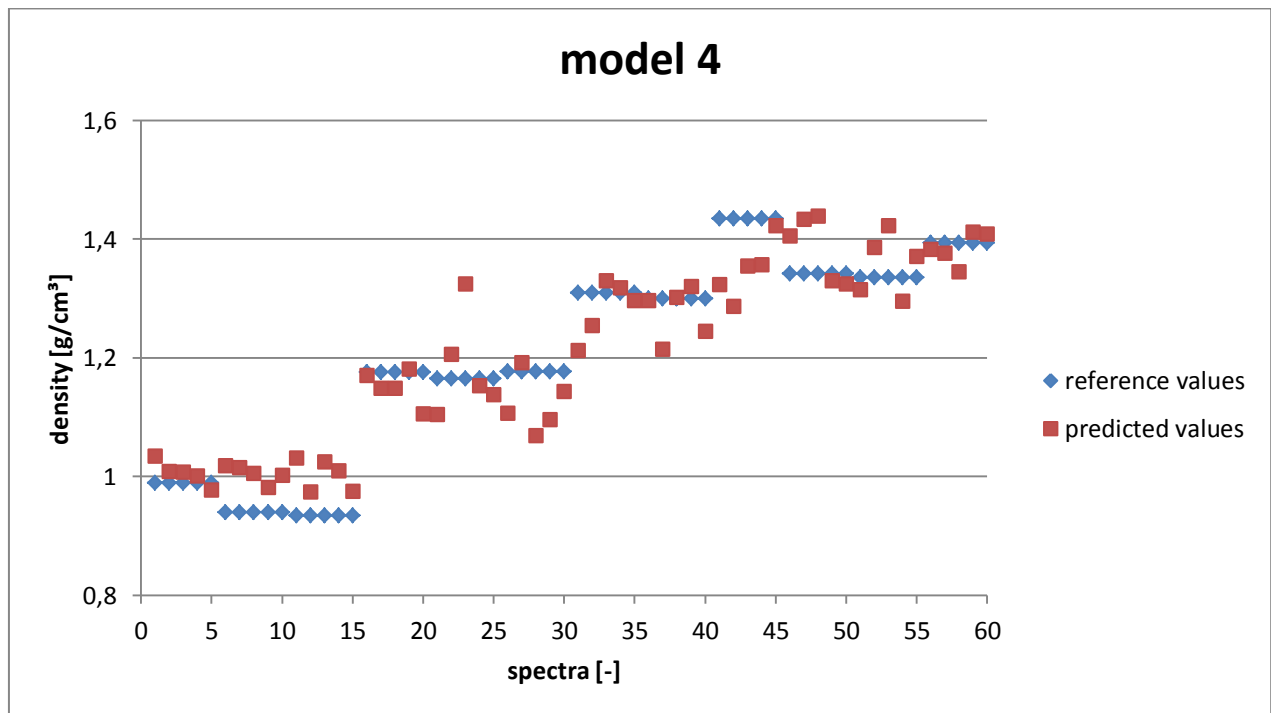


Figure 43: Final PLS-model from OPUS for Avicel PH 102 with a RMSEP of 0,061, a BIAS of 0,001 and a RSEP of 5,002%. The force was 3, 7, 9 and 13kN and the gap was constant at 1mm. Blue colored are the reference values and red the predicted values. 15 spectra were recorded from each trial, and the graph thus has a total of 60 predicted values. Three density measurements were made for each trial, therefore three reference values for each trial.

Table 13: Data analysis of model 4

RMSEP [-]	BIAS [-]	RSEP [%]
0,061	0,001	5,002

Table 14: Data analysis of each trial

Trial Nr. [-]	RMSEP [-]	BIAS [-]	RSEP [%]
01	0,059	0,050	6,136
03	0,065	0,020	5,500
06	0,069	0,046	5,078
07	0,051	0,020	3,754

6.6.6.4. Final PLS-model from SIMCA for Avicel PH 102

The best PLS-model developed with SIMCA was in wavelength region 1100-1650 nm with an RSEP of 9,284 % (see Figure 44 and Table 15). The RSEP was then also calculated again for various density steps. The results showed that the theory, which says that the RSEP is decreasing with higher density, was wrong (see Table 16). However, the RSEP was at the highest density still the lowest.

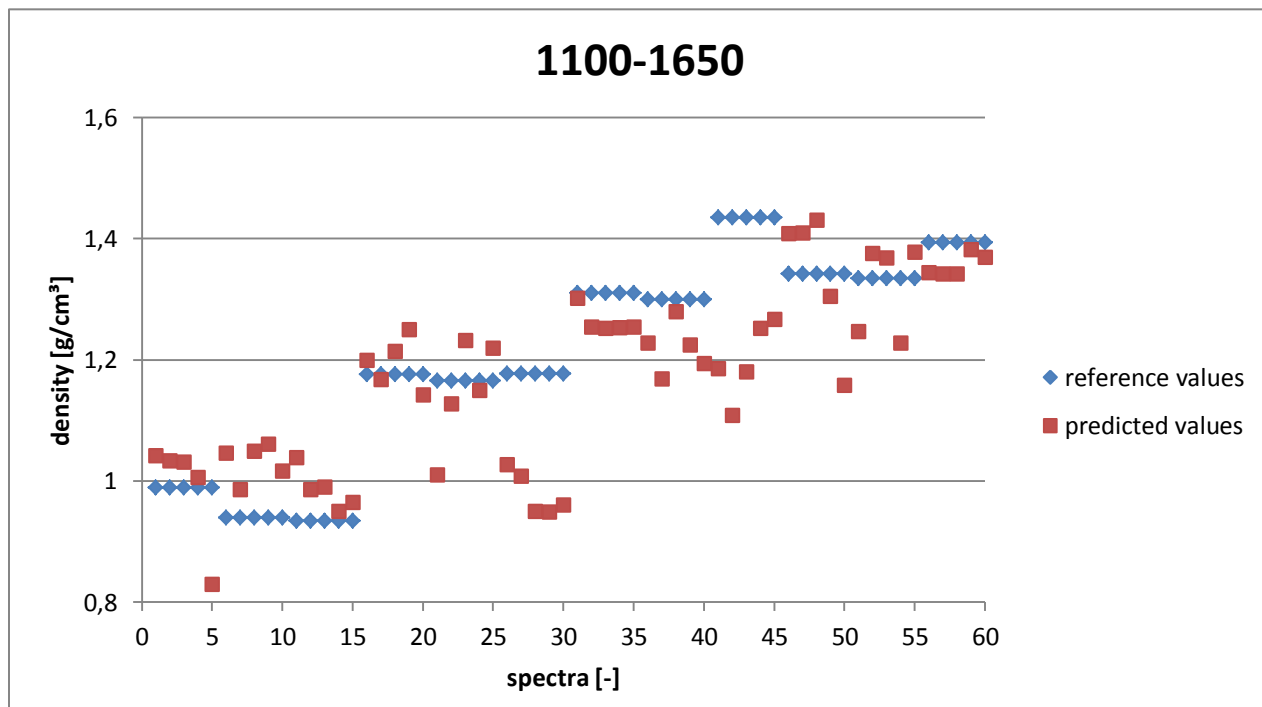


Figure 44: Final PLS-model from SIMCA for Avicel PH 102 within the wavelengths 1100-1650nm, with a RMSEP of 0,179, a BIAS of -0,039 and a RSEP of 9,284%. The force was 3, 7, 9 and 13kN and the gap was 1mm. Blue colored are the reference values and red the predicted values. 15 spectra were recorded from each trial, and the graph thus has a total of 60 predicted values. Three density measurements were made for each trial, therefore three reference values for each trial.

Table 15: Data analysis of the PLS-model in range 1100-1650

RMSEP [-]	BIAS [-]	RSEP [%]
0,179	-0,039	9,284

Table 16: Data analysis of each trial for the SIMCA model

Trial Nr. [-]	RMSEP [-]	BIAS [-]	RSEP [%]
01	0,080	0,048	8,376
03	0,127	-0,066	10,848
06	0,152	-0,121	11,260
07	0,075	-0,018	5,521

6.6.6.5. Score plots with SIMCA for Avicel PH 102

To get a more detailed view of the PLS-model, the PLS of the wavelengths 1496-1650nm is shown in two different score plots and a plot of the regression line. The first plot, shown in Figure 45, is for calibration, and shows the area where the model is valid. The ellipse describes data with a confidence interval of 95%. In addition, you can see a density trend. From left to right and from blue to orange the density values are increasing. A few outliers are also visible in the graph. The reason for that were inaccurate density values from the GeoPyc.

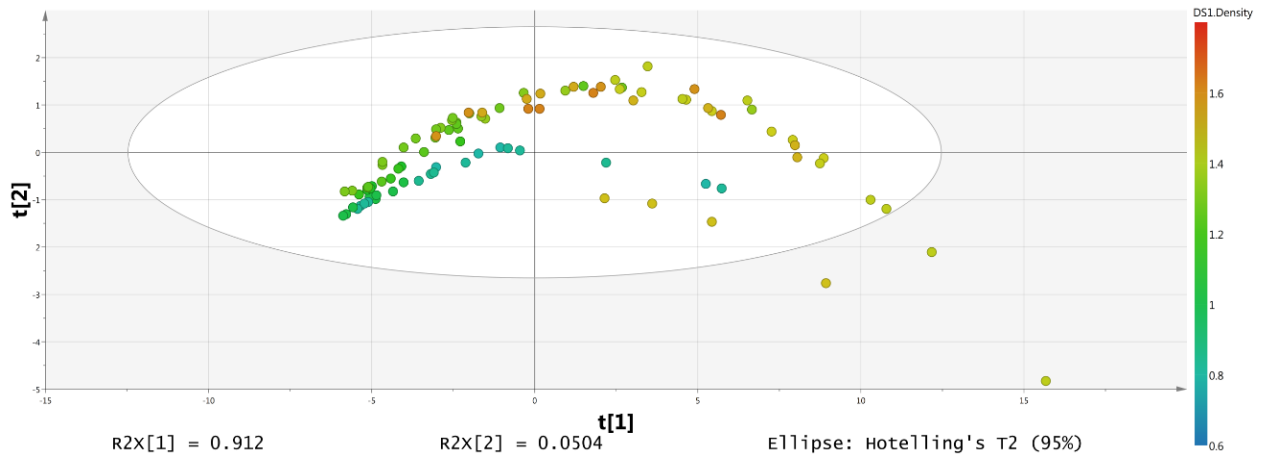


Figure 45: PLS-calibration score plot with SIMCA for Avicel PH 102, the ellipse describes data with a confidence interval of 95%. In addition, you can see a trend of the density values. From left to right the density increases. Also marked with the colors blue, green yellow and orange, with a value of 0.6, 1, 1.4 and 1.5

The second diagram represents the values of the test spectra with the calibration values in the same space (see Figure 46). In red are the values from the calibration model and blue is the prediction set. The trend in the graph showed that the predicted values follow the values from the calibration set, therefore this prediction is reproducible.

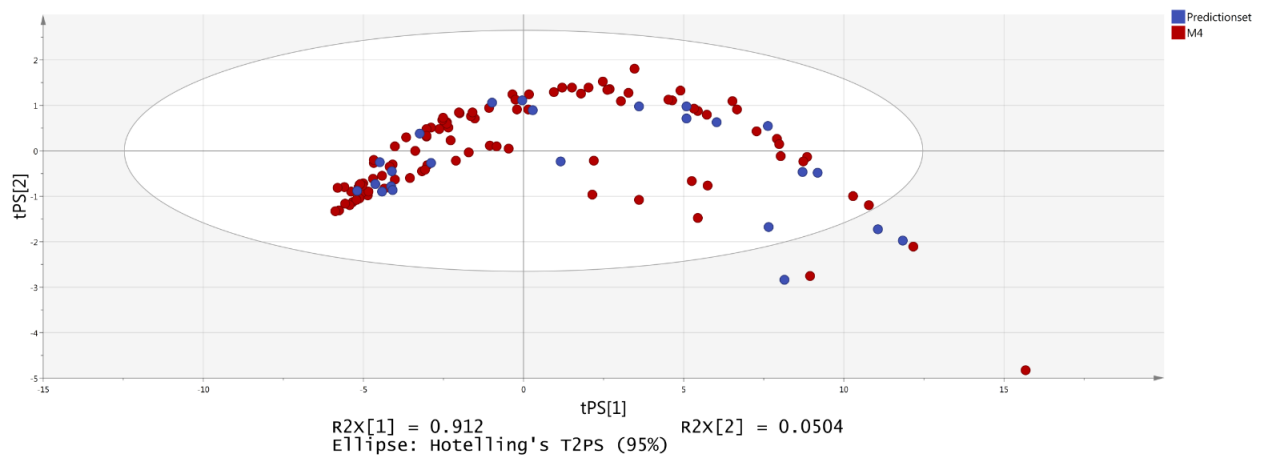


Figure 46: PLS-score plot with SIMCA for Avicel PH 102, red = values of the calibration model, blue = predicted values. Prediction set follows the values of calibration model, therefore these models show reproducible prediction.

In order to get a more detailed view of the relation between the calibration values and the prediction, the plot of the regression line is shown (see Figure 47). The x-axis represents the density prediction of the model and the y-axis the density reference values from GeoPyc. The closer the points are to the straight line, the more accurate are the predicted values. On the line, the predicted value and the reference value are the same.

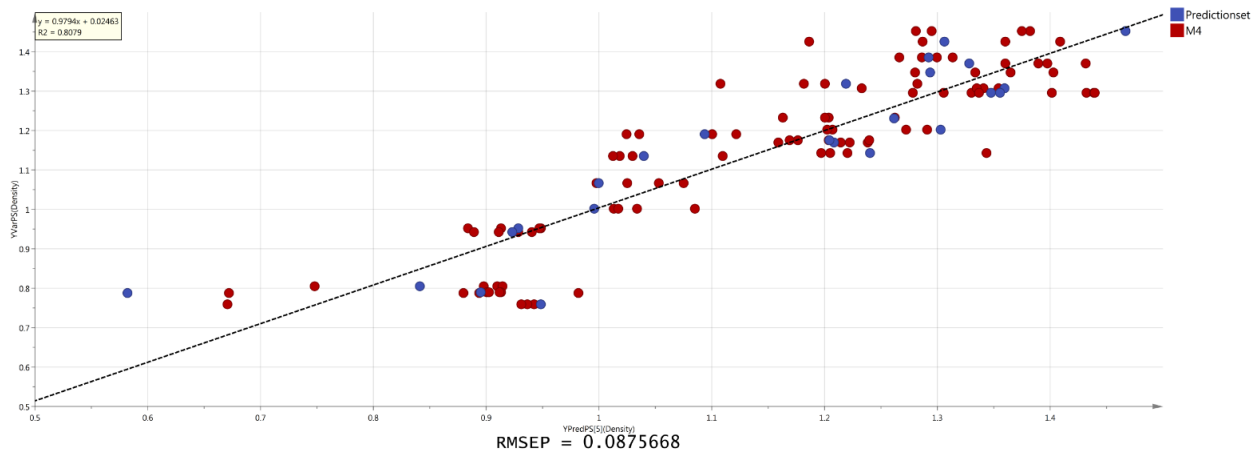


Figure 47: SIMCA plot of the regression line of the prediction set (blue) and the values from the calibration set (red) for Avicel PH 102 between the wavelengths 1496 and 1650nm, the closer the points are to the straight line, the more accurate are the predicted values. On the line, prediction is equal to the observed values.

6.7. Experiment 04 (Verification of Experiment 03)

To see whether the aforementioned experiment 03 is reproducible, the entire experiment was performed with Prosolv again. For this experiment only the spectra from Bruker have been analyzed further, since experiment 03 showed that both spectrometer (Bruker and MicroNIR) lead to similar results. Out of 4 models, the PLS model named model1 with an RSEP of 11.156% was considered the best because it had the lowest RSEP (see Figure 48). Compared to the RSEP of 6,164 % for Avicel PH 102 (see section 6.6.6.1) it was less accurate, but was still considered acceptable.

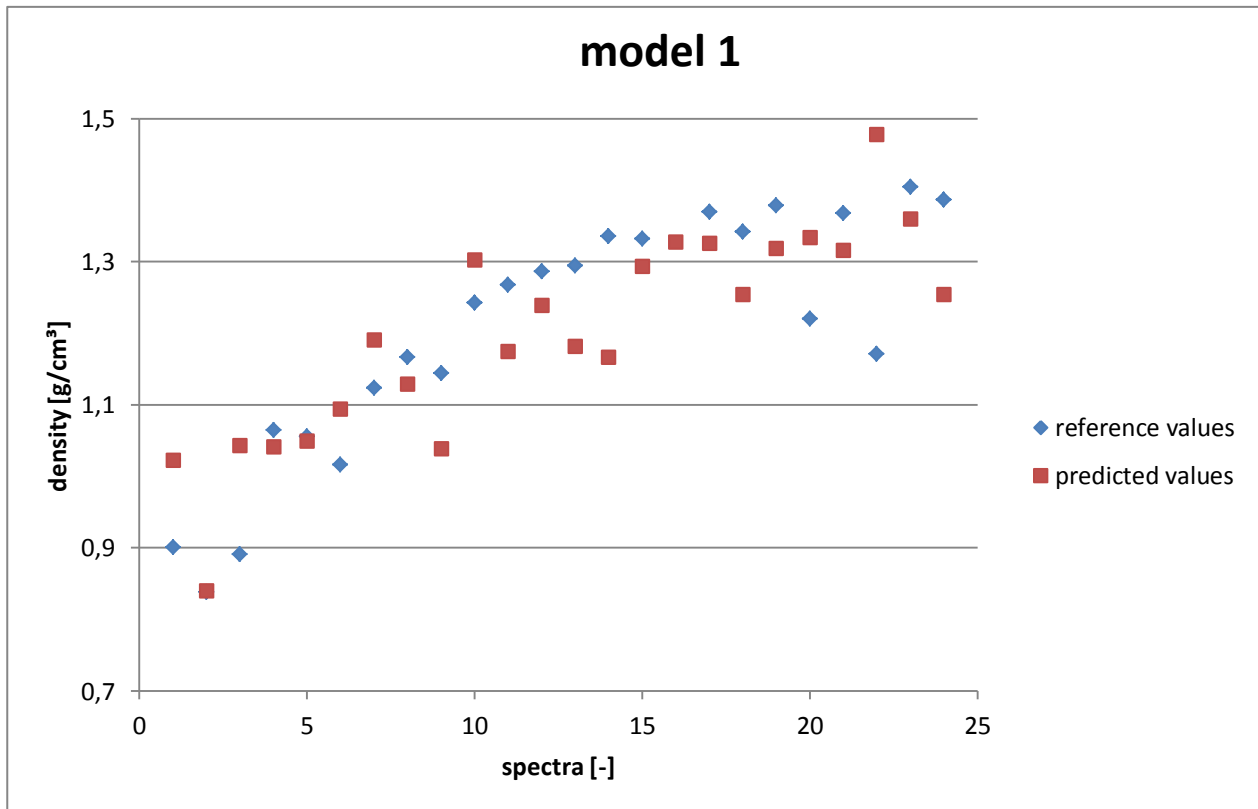


Figure 48: PLS-model for Prosolv with a RMSEP of 0,138, a BIAS of -0,025 and a RSEP of 11,156%. Compared to the RSEP of 6,164% from the PLS-model for Avicel PH 102 this RSEP was a little bit high but still it was a good result. The reason for the high RSEP was the inaccurate density values.

From the trials 01, 03, 04 and 06, new spectra and density values were recorded or calculated and then linked to verify the old model. This time the model3 with a RSEP of 14,901 % was the best. Compared to a RSEP of 5,002 % of the model made for Avicel PH 102, see section 6.6.6.3, the RSEP value was too high. As can be seen in Figure 49, there was a mistake in the density measurement of trial 07. The reason for that were inaccurate density values from GeoPyc, therefore the RSEP was then calculated for all different trials (see Table 17). To optimize the model the wrong density value of trial 07 was replaced with the average of the correct ones. The RSEP of trial 07 decreased from 19,122 % to 9,486% (see yellow marked cells in Table 17 and Table 18), and therefore the RSEP of the whole model was 12,239% only.

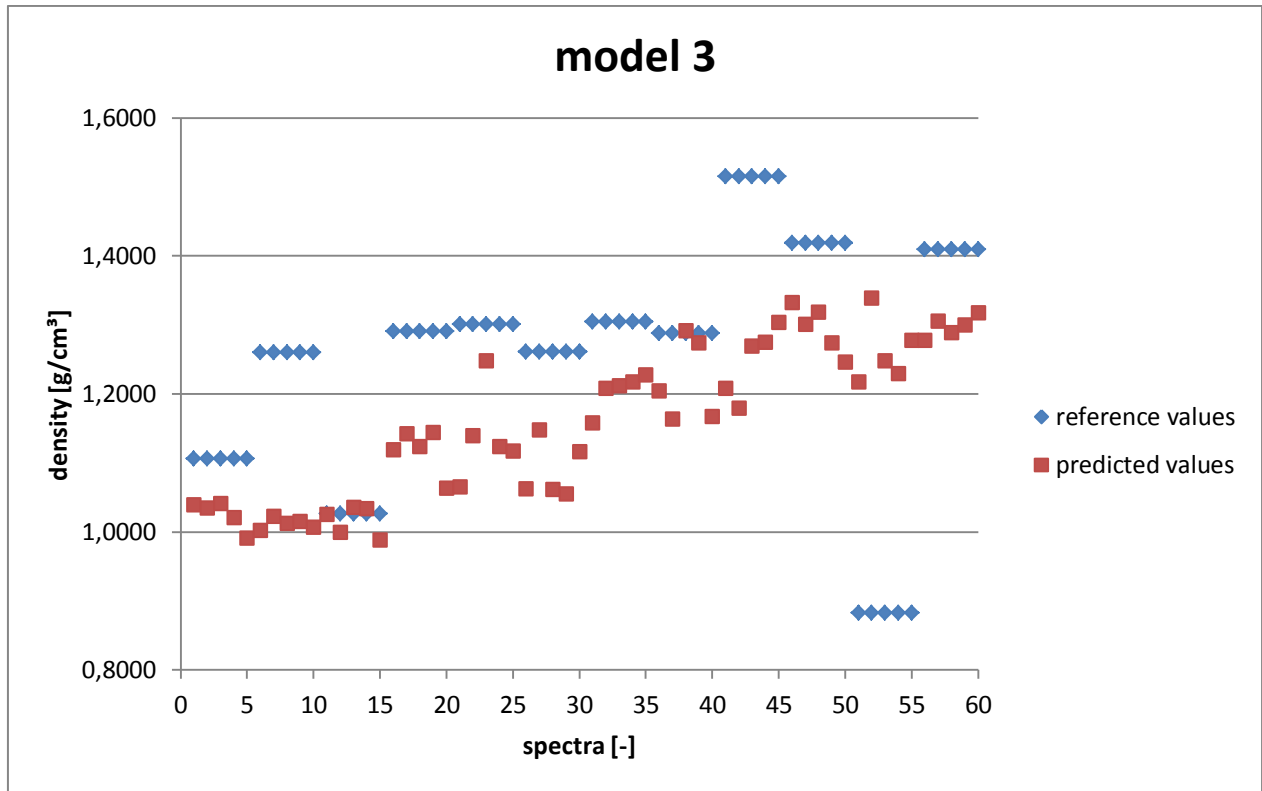


Figure 49: Final PLS-model for Prosolv with a RMSEP of 0,189, a BIAS of -0,095 and a RSEP of 14,901%. The reason for the increased RSEP was that the density value of trial 07 was incorrect. To get a better model the wrong value could be replaced. In addition, some other densities were inaccurate and can also be replaced in the future.

Table 17: Data analysis of each trial for the PLS model for Prosolv without optimization of the density values

Trial Nr. [-]	RMSEP [-]	BIAS [-]	RSEP [%]
01	0,152	-0,113	13,368
03	0,175	-0,169	13,609
06	0,175	-0,145	12,748
07	0,241	0,048	19,122

Table 18: Data analysis of each trial for the PLS model for Prosolv with optimization of the density values

Trial Nr. [-]	RMSEP [-]	BIAS [-]	RSEP [%]
01	0,152	-0,113	13,368
03	0,175	-0,169	13,609
06	0,175	-0,145	12,748
07	0,134	-0,129	9,486

7. Summary

A PLS-model for predicting the density of roller compacted ribbons was constructed and tested for Avicel PH 102 and Prosolv. Two spectrometers collected spectra of the ribbons, namely the Matrix F from Bruker and the MicroNir from Viavi Solutions Inc. The ribbons were produced with various machine parameters with the roller compactor BRC 25 from Bohle. The gap was constant at 1mm, the roller speed was always 10 rpm and the dosing percentage was adjusted to 100%. Only the force changed from 1kN to 3, 5, 7, 9, 11, 13 and 15kN. Therefore, a total of 8 trials were created. Spectra were recorded from all trials and their density was determined using a GeoPyc. These values were then combined to obtain a PLS model. The software OPUS was used for the Matrix F spectra and SIMCA was used for the spectra of the MicroNir. In order to find these machine settings and a good setup, some preliminary tests had to be carried out.

One of the biggest challenges was the determination of ribbons density. In order to obtain suitable values, 3 different methods were tested. Since the caliper and the oil method were too inaccurate, a new method had to be found. With the help of the GeoPyc, precise and reproducible results were achieved (see section 3.2.)

The second phase was to gain experience with the roller compactor and to find the best machine settings. This was very time-consuming, because some powders were very cohesive, sensitive to moisture or had a very small particle size, which lead to wall adhesion, and consequently, prevented the feeding screw from moving forward and therefore the machine has to be stopped and cleaned manually (see section 6.4).

The next phase was the handling of the Near Infrared Spectrometers. This was also very challenging, because predicting density of roller compacted ribbons with NIR-spectroscopy was unique according to our best knowledge and research (see chapter 4. and section 6.5)

The PLS-models for Avicel PH 102 developed using OPUS and SIMCA (see Figure 43 and Figure 44) with a RSEP of 5,002% and 9,284%, respectively, showed that these models were very accurate and can be used in future. To confirm this result, a PLS-model for Prosolv was developed (see Figure 48 and Figure 43). Since the PLS-models with the Matrix F and the MicroNir showed almost the same results, for the Prosolv the models were built with the Matrix F spectra only. The RSEP of 14,91% seemed to be too high, but a closer evaluation showed that only the density measurement was inaccurate for some trials. Therefore, the PLS-model for Prosolv confirmed that predicting the density of the ribbons with NIR-spectroscopy is possible. Furthermore the experiments showed which material properties and machine settings were decisive for the roller compactor process. In future, this thesis of predicting density of roller compacted ribbons can be used as a framework to create a model for the entire roller compactor process.

8. References

1. Hsu SH, Reklaitis G V., Venkatasubramania V. Modeling and control of roller compaction for pharmaceutical manufacturing: Part II: Control system design. *J Pharm Innov.* 2010;5(1-2):24-36. doi:10.1007/s12247-010-9077-z.
2. Micromeritics Instrument Corp. AccuPyc II 1340 | Micromeritics. <http://www.micromeritics.com/Product-Showcase/AccuPyc-II-1340.aspx>. Accessed May 4, 2017.
3. Micromeritics Pharmaceutical Services. About | Micromeritics Pharmaceutical Services. <http://micrx.com/About.aspx>. Accessed May 4, 2017.
4. Micromeritics. GeoPyc 1360 Envelope Density Analyzer. 2014:2. http://www.micromeritics.com/Repository/Files/GeoPyc_1360_reg_and_TAP.pdf.
5. Process Sensors Corp. Near Infrared Measurements – How Do They Work? - Welcome to PSC's Blog! http://www.processsensors.com/appbl_II/?p=2998. Accessed May 5, 2017.
6. Blanco M, Villarroya I. NIR spectroscopy: A rapid-response analytical tool. *TrAC - Trends Anal Chem.* 2002. doi:10.1016/S0165-9936(02)00404-1.
7. Thermo Nicolet Corporation. FT-IR vs. Dispersive Infrared: Theory of Infrared Spectroscopy Instrumentation. *A Thermo Electron Bus.* 2002:2. http://www.thermo.com/eThermo/CMA/PDFs/Product/productPDF_21611.pdf.
8. Otsuka M, Tanabe H, Osaki K, Otsuka K, Ozaki Y. Chemoinformetrical evaluation of dissolution property of indomethacin tablets by near-infrared spectroscopy. *J Pharm Sci.* 2007. doi:10.1002/jps.20704.
9. Román-Ospino AD, Singh R, Ierapetritou M, et al. Near infrared spectroscopic calibration models for real time monitoring of powder density. *Int J Pharm.* 2016;512(1):61-74. doi:10.1016/j.ijpharm.2016.08.029.
10. Multivariate_data_analysis_wiki.
11. Williams LJ. Principal component analysis. 2010;2(August). doi:10.1002/wics.101.
12. Godoy JL, Vega JR, Marchetti JL. Relationships between PCA and PLS-regression. *Chemom Intell Lab Syst.* 2014;130:182-191. doi:10.1016/j.chemolab.2013.11.008.
13. Scheibelhofer O, Balak N, Wahl PR, Koller DM, Glasser BJ, Khinast JG. Monitoring Blending of Pharmaceutical Powders with Multipoint NIR Spectroscopy. *AAPS PharmSciTech.* 2013;14(1):234-244. doi:10.1208/s12249-012-9910-4.
14. The absolute and relative densities of pharmaceutical solids play an important role in determining their performance (e.g.
15. Analyzer ED. GeoPyc 1365[®].